Mon. Not. R. Astron. Soc. **358,** 1290–1308 (2005) doi:10.1111/j.1365-2966.2005.08784.x

Stellar contents of two young open clusters: NGC 663 and 654

A. K. Pandey,[1⋆] K. Upadhyay,[1] K. Ogura,[2] Ram Sagar,[1] V. Mohan,[1] H. Mito,[3] H. C. Bhatt[4] and B. C. Bhatt[4]

[1]*Aryabhatta Research Institute of Observational Sciences, Manora Peak, Naini Tal, 263 129, Uttaranchal, India*
[2]*Kokugakuin University, Higashi, Shibuya-ku, Tokyo 150-8440, Japan*
[3]*Kiso Observatory, School of Science, University of Tokyo, Mitake-mura, Kiso-gun, Nagano 397-0101, Japan*
[4]*Indian Institute of Astrophysics, Bangalore 560034, India*

Accepted 2005 January 5. Received 2004 December 22; in original form 2004 March 3

ABSTRACT

UBVRI CCD photometry in a wide field around two young open clusters, NGC 663 and 654, has been carried out. Hα and polarimetric observations for the cluster NGC 654 have also been obtained. We use the photometric data to construct colour–colour and colour–magnitude diagrams, from which we can investigate the reddening, age, mass and evolutionary states of the stellar contents of the these clusters. The reddening across the cluster regions is found to be variable. There is evidence for anomalous reddening law in both clusters; however, more infrared and polarimetric data are needed to conclude about the reddening law. Both clusters are situated at about a distance of 2.4 kpc. Star formation in both clusters is found to be a continuous process. In the case of NGC 663, star formation seems to have taken place sequentially, in the sense that formation of low-mass stars precedes the formation of most massive stars. Whereas, in the case of NGC 654, formation of low-mass stars did not cease after the formation of most massive stars in the cluster.

Key words: stars: formation – stars: luminosity function, mass function – dust, extinction – galaxies: star clusters.

1 INTRODUCTION

Star clusters are useful objects to study the star formation process. To understand the star formation process, it is necessary to know how the star formation proceeds in star clusters and whether the stellar mass distribution that arises from the fragmentation of molecular cloud is the same for different molecular clouds. It is also important to study whether the star formation process depends on the local conditions of the different parts of the Galaxy. Among various tools, the initial mass function (IMF) is one of the most important tools to study the above-mentioned questions. One of the major uncertainties in the studies of the IMF is the issue whether the IMF is universal or determined by environmental effects. Scalo (1998) cited much evidence that does not support a universal IMF; on the other hand, Kroupa (2001) does not find convincing evidence for a variable IMF.

Dynamical evolution and mass segregation can have a significant effect on the radial structure as well as on the shape of the present-day mass function (MF) of open clusters (see, for example, Pandey et al. 2001). Although, as per standard theory where stars in clusters evolve rapidly towards a state of energy equipartition through stellar encounters, consequently mass segregation – in the sense that more massive stars tend to lie near the centre – is well accepted. However, observations of mass segregation in very young clusters (e.g. Pandey, Mahara & Sagar 1992; Hillenbrand 1997) suggest that in the case of a few young clusters the mass segregation may be the imprint of star formation process itself.

An important study to explore the star formation history and IMF of young open clusters was by Phelps & Janes (1994, hereafter PJ94), who observed 23 open clusters in the Cassiopeia region and estimated IMFs for eight young clusters (Phelps & Janes 1993). However, most studies of open clusters, including those of Phelps & Janes (1993) and PJ94, are based on the central region of the star clusters. A recent study of the structure of open clusters by Nilakshi et al. (2002) indicates that most open clusters have extended region (known as corona). Pandey, Mahara & Sagar (1990) also support the existence of corona around open clusters. The corona of star clusters, which usually contains faint and low-mass stars, has not been studied in detail because of the non-availability of photometry of stars in that region. We have undertaken a CCD photometric study of a large area around open clusters using the 2K $\times$ 2K CCD mounted on the 105-cm Schmidt telescope of the Kiso Observatory, which gives a $\sim$50-arcmin^2 field, and the 1K $\times$ 1K CCD mounted on the 104-cm telescope of the State Observatory, Nainital, which gives a $\sim$6-arcmin^2 field. The first paper of the programme was on the cluster NGC 7654 (Pandey et al. 2001), which indicates that a uniform MF cannot be applied for different regions in the cluster. In this paper, we present wide field CCD photometry carried out around young open clusters, NGC 663 and 654.

⋆E-mail: pandey@upso.ernet.in

The open cluster NGC 663 ($\alpha_{2000} = 01^h46^m09^s$, $\delta_{2000} = 61^\circ14'06''$, $l = 129\overset{\circ}{.}46$, $b = -0\overset{\circ}{.}99$, Trumpler class II3r) is located in the Cassiopeia region. The central region of the cluster NGC 663 has been studied widely by various authors. The *UBV* photographic/photoelectric photometries have been reported by (Hoag et al. 1961, hereafter H61), McCuskey & Houk (1964), Moffat & Vogt (1974) and van den Bergh & de Roux (1978), whereas Tapia et al. (1991) carried out near-infrared and Strömgren photometry of the central part of NGC 663. PJ94 have reported *UBV* CCD photometry of the cluster in a field of $\sim$19.5 $\times$ 19.5 arcmin^2. Recently, Pigulski, Kopacki & Kolaczkowski (2001, hereafter P01) have reported a $BV(RI)_C$ Hα photometry for a 14 $\times$ 20 arcmin^2 field of the cluster NGC 663.

The open cluster NGC 654 ($\alpha_{2000} = 01^h44^m00^s$, $\delta_{2000} = 61^\circ53'06''$, $l = 129\overset{\circ}{.}09$, $b = -0\overset{\circ}{.}35$, Trumpler class II2r) is located near NGC 663 in the Cassiopeia region. The cluster has been studied photometrically several times (e.g. Pesch 1960, H61, McCuskey & Houk 1964; Moffat 1972; Samson 1975; Stone 1980; Joshi & Sagar 1983, hereafter JS83). The CCD photometry of the NGC 654 in a field of $\sim$6.6 $\times$ 6.6 arcmin^2 was carried out by PJ94.

The radial density profiles for the clusters NGC 663 and 654, derived by Nilakshi et al. (2002) using the Digitized Sky Survey (DSS), indicate diameters of $\sim$27 and $\sim$20 arcmin, respectively. None of the studies reported earlier covers the entire region of the clusters. This present study is an effort to study the clusters NGC 663 and 654 in detail.

2 OBSERVATIONS AND DATA REDUCTION

2.1 NGC 663

The CCD $UBVI_C$ data were acquired in 1999 November using the 2048 $\times$ 2048 pixel^2 CCD camera mounted on the 105-cm Schmidt telescope of the Kiso Observatory. At the Schmidt focus ($f/3.1$) each pixel corresponds to 1.5 arcsec and the entire chip covers a field of $\sim$50 $\times$ 50 arcmin^2 on the sky (for details, see Pandey et al. 2001). The FWHM of the star images was $\sim$4 arcsec. The log of observations is given in Table 1. A number of bias and dome flat frames were also taken during the observing runs. To standardize the observations, we generated secondary standards in the field of NGC 663 by observing SA 98 field of Landolt (1992) using the 104-cm Sampurnanand telescope of the State Observatory, Naini Tal.

2.2 NGC 654

The CCD BVI_C and Hα observations were carried out in 1993 October–November and in 1998 December, respectively, using the 1024 $\times$ 1024 pixel^2 CCD camera mounted on the $f/13$ Cassegrain focus of the 104-cm Sampurnanand telescope of the State Observatory, Naini Tal. In this set-up, each pixel of the CCD corresponds to 0.37 arcsec and the entire chip covers a field of $\sim$6 $\times$ 6 arcmin^2 on the sky. To improve the signal-to-noise (S/N), the observations were taken in the binning mode of 2 $\times$ 2 pixel. The FWHM of the star images was $\sim$2 arcsec. The log of observations is given in Table 1. A number of bias and twilight flat-field frames were also taken during the observing runs. The standardization of observations was carried out using the Landolt (1992) stars.

2.3 Blank field

A common blank field ($\sim$6 $\times$ 6 arcmin^2) in the VI_C passband at a distance of $\sim$40 arcmin towards the north from the centre of NGC 663 and $\sim$30 arcmin towards the east from the centre of NGC 654 was also observed. The observations were carried out on 1993 October 16 using the 1024 $\times$ 1024 pixel^2 CCD camera mounted on the $f/13$ Cassegrain focus of the 104-cm Sampurnanand telescope of the State Observatory, Naini Tal. The log of observations is given in Table 1.

Table 1. Log of observations.

Cluster	Filter	Exposure time (s)	No. of frames	Date (yyyy.mm.dd)
NGC 663	*U*	60	9	1999.11.03
	U	180	9	1999.11.03
	B	20	8	1999.11.03
	B	60	3	1999.11.03
	V	10	8	1999.11.03
	V	60	3	1999.11.03
	I	10	12	1999.11.03
	I	60	8	1999.11.03
NGC 654	*B*	60	3	1993.10.09
North-west	*B*	600	4	1993.10.09
	V	30	3	1993.10.09
	V	300	3	1993.10.09
	R	20	3	1993.10.09
	R	150	3	1993.10.09
	I	20	3	1993.10.09
	I	150	3	1993.10.09
	Hα	300	3	1998.12.09
	Hα	1200	3	1998.12.09
NGC 654	*B*	60	3	1993.10.09
North-east	*B*	600	4	1993.10.09
	V	30	3	1993.10.09
	V	300	3	1993.10.09
	R	20	3	1993.10.09
	R	150	3	1993.10.09
	I	20	3	1993.10.09
	I	150	3	1993.10.09
	Hα	300	3	1998.12.09
	Hα	1200	3	1998.12.09
NGC 654	*B*	60	3	1993.11.10
South-east	*B*	600	4	1993.11.10
	V	30	3	1993.11.10
	V	300	4	1993.11.10
	R	20	3	1993.11.10
	R	150	3	1993.11.10
	I	20	3	1993.11.10
	I	150	3	1993.11.10
	Hα	300	3	1998.12.09
	Hα	900	3	1998.11.12
NGC 654	*B*	60	3	1993.11.10
South-west	*B*	600	4	1993.11.10
	V	30	3	1993.11.10
	V	300	4	1993.11.10
	R	20	3	1993.11.10
	R	150	3	1993.11.10
	I	20	3	1993.11.10
	I	150	3	1993.11.10
	Hα	300	3	1998.12.09
	Hα	900	3	1998.11.12
Blank field	*V*	30	3	1993.10.16
	V	300	3	1993.10.16
	I	10	3	1993.10.16
	I	300	3	1993.10.16

Table 2. The photometric data of the stars in the field of NGC 663. X, Y are the pixel coordinates. Radius is with respect to the centre $X = 934$, $Y = 887$.

No.	X	Y	V	U–B	B–V	V–I	Radius (arcsec)
1	932.13	886.73	17.527	–	1.051	1.490	2.834
2	928.44	880.90	15.581	0.531	0.707	0.933	12.381
3	933.42	876.60	18.738	–	1.194	1.700	15.624
4	941.96	896.79	20.424	–	1.302	2.974	18.927
5	945.92	893.09	20.378	–	–	2.140	20.078

The image processing was carried out at the State Observatory, Naini Tal, using the European Southern Observatory (ESO) MIDAS software package. Different clean frames of same exposure time and filters were co-added. The photometric measurements of the stars were performed using the DAOPHOT II profile fitting software. The stellar images were well sampled and a variable point spread function (PSF), evaluated from several uncontaminated stars present in the frame, was applied. When brighter stars were saturated on deep-exposure frames, their magnitudes were taken from short-exposure frames. Stars brighter than $V \sim 10$ could not be measured in both clusters because they were saturated even in the short-exposure frames. The image parameters and errors provided by DAOPHOT were used to reject poor measurements. The photometric data along with position of the stars measured in the cluster are given in Tables 2 and 3 for the clusters NGC 663 and 654, respectively; these are available in electronic form only. The format of the table is shown below. The DAOPHOT errors and the difference of input and output magnitudes of the artificial stars (generated using the ADDSTAR routine; see Section 4) were used to estimate the observational errors at each magnitude bin. The larger mean value of the error at each magnitude bin obtained by using the above-mentioned methods is adopted and these are given in Table 4.

3 COMPARISON WITH THE PREVIOUS PHOTOMETRIES

Figs 1 and 2 display a comparison of the present CCD photometry with the previous reported photoelectric photometry (NGC 663 and 654 by H61; NGC 654 by JS83) and CCD photometry (NGC 663 and 654 by PJ94; NGC 663 by P01). The difference Δ(present data − literature) is plotted as a function of V magnitude in Figs 1 and 2 for NGC 663 and 654, respectively, and statistical results are given in Table 5.

In the case of NGC 663, the comparison indicates the following.

(i) The V magnitudes obtained by us are in agreement with those given by PJ94, whereas the V magnitudes obtained by us are fainter by ∼0.1 mag in comparison to those obtained by H61. The V magnitudes of brighter stars ($V < 15$) obtained in the present work are in agreement with those given by P01. However, the V magnitudes of stars fainter than $V \sim 15$ show a trend with increasing V magnitude, in the sense that present estimation becomes fainter.

(ii) The $(B–V)$ colours given by PJ94 are in good agreement with those obtained in the present work, whereas the $(B–V)$ colours given by H61 are redder by ∼0.1 mag. The $(B–V)$ colours for stars $V \leqslant 14$ obtained in the present work are bluer than those given by P01. The $(B–V)$ colours given by P01 show a blueward trend in $\Delta(B–V)$ with increasing V magnitude.

(iii) The $(U–B)$ colours given by H61 are reddened by ∼0.04 mag in comparison to those obtained in the present work. The $(U–B)$ colour for stars $V \leqslant 15$ given by PJ94 are in good agreement with the $(U–B)$ colour obtained in the present work. However, $(U–B)$ colours for stars having $V > 15$, given by PJ94, show a blueward trend in $\Delta(U–B)$ with increasing V magnitude.

(iv) The $(V–I)$ colours reported by P01 show a blueward trend in $\Delta(V–I)$ with increasing V magnitude.

A comparison of various published photoelectric and photographic measurements of NGC 654 have been carried out by Huestamendia, del Rio & Mermelliod (1993). A comparison of present CCD photometry with the CCD photometry of PJ94 and photoelectric photometry of JS83 indicates the following.

(i) The V magnitudes obtained in the present study are in good agreement with those reported by PJ94, whereas the V magnitudes ($11 \leqslant V \leqslant 15$) given by JS83 are fainter by ∼0.08 in comparison to the V magnitudes obtained in the present study.

(ii) The $(B–V)$ colours given by PJ94 for $11 \leqslant V \leqslant 18$ and by JS83 for stars having $11 \leqslant V \leqslant 15$ are in agreement with those

Table 4. Average photometric errors (σ) as a function brightness in the cluster region.

Magnitude range		σ_U	σ_B	σ_V	σ_R	σ_I
NGC 663	$\leqslant 14$	0.02	0.02	0.02		0.03
	14–15	0.02	0.03	0.03		0.04
	15–16	0.03	0.03	0.04		0.04
	16–17	0.03	0.04	0.04		0.05
	17–18	0.04	0.04	0.04		0.06
	18–19	0.06	0.04	0.06		0.08
	19–20	0.09	0.06	0.09		0.11
NGC 654	$\leqslant 14$		0.01	0.01	0.01	0.01
	14–15		0.01	0.01	0.01	0.02
	15–16		0.01	0.01	0.02	0.02
	16–17		0.02	0.02	0.03	0.03
	17–18		0.03	0.02	0.05	0.04
	18–19		0.04	0.03	0.06	0.05
	19–20		0.06	0.05	0.07	0.08
	20–21			0.08	0.09	0.09

Table 3. The photometric data of the stars in the field of NGC 654. X, Y are the pixel coordinates. Radius is with respect to the centre $X = 425$, $Y = 500$.

NO.	X	Y	V	B–V	V–R	V–I	Hα	R–Hα	Radius (arcsec)
1	416.37	497.51	17.237	1.039	0.656	1.088	16.676	−0.095	8.982
2	429.17	511.96	18.143	1.412	1.126	2.035	17.181	−0.164	12.666
3	425.62	486.56	14.272	0.903	0.402	1.059	14.268	−0.399	13.454
4	438.32	503.32	15.196	0.913	0.461	1.195	14.833	−0.098	13.728
5	440.32	492.42	12.108	0.724	0.476	1.038	11.621	0.011	17.093

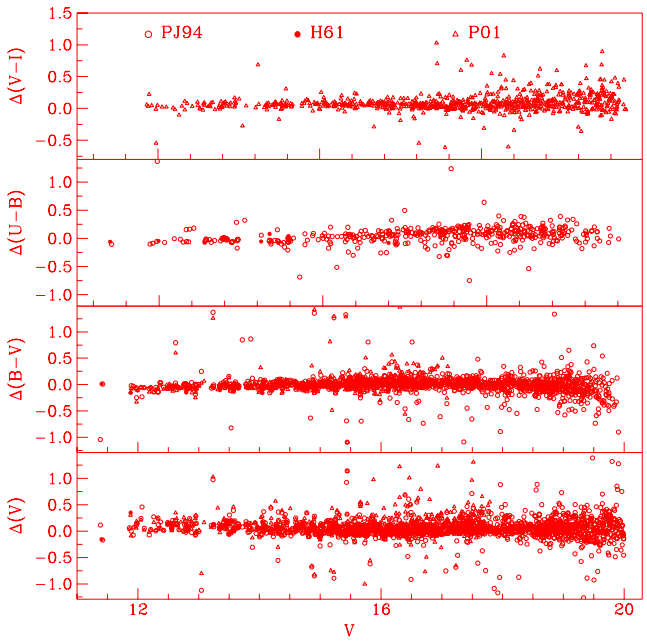

Figure 1. Comparison of the present CCD photometry of NGC 663 with the photoelectric photometry by H61 and with the CCD photometries by PJ94 and P01.

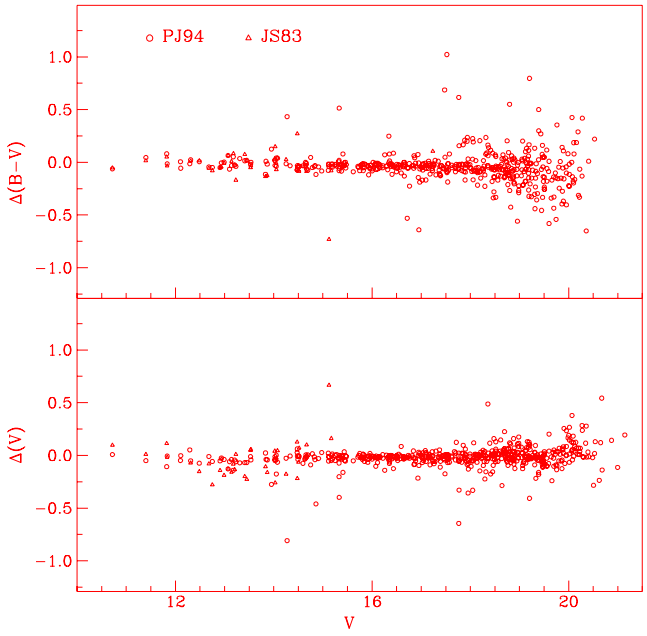

Figure 2. Comparison of the present CCD photometry of NGC 654 with the photoelectric photometry by JS83 and with the CCD photometry by PJ94.

obtained in the present work. However, $(B–V)$ colours given by PJ94 for stars fainter than $V \sim 18$ are redder in comparison to those obtained in the present work.

4 COMPLETENESS OF THE PHOTOMETRIC DATA

The incompleteness in the data may occur for various reasons (e.g. crowding of the stars). A quantitative evaluation of the completeness of the photometric data with respect to the brightness and the position on a given frame is necessary because it is necessary to convert the observed luminosity function (LF) to a true LF. We used the ADDSTAR routine of DAOPHOT II to determine the completeness factor (CF). The procedure has been outlined in detail in our earlier work (Pandey et al. 2001). Briefly, we randomly added artificial stars to both V and I images in such a way that they have similar geometrical locations but differ in I brightness according to mean $(V–I)$ colour of the main-sequence (MS) stars. The luminosity distribution of artificial stars is chosen in such a way that more stars are inserted towards the fainter magnitude bins. The frames are rereduced using the same procedure used for the original frame. The ratio of the number of stars recovered to those added in each magnitude interval gives the CF as a function of magnitude. The minimum value of the CF of the pair (i.e. V- and I-band observations), given in Table 6, is used to correct the data for incompleteness. The incompleteness of the data increases with increasing magnitude as expected.

5 RADIAL STRUCTURE OF THE CLUSTER

The area covered by present CCD observations is sufficiently large for studying the radial structure of the clusters. The stellar distribution in a ±40-pixel-wide strip around the eye estimated centre is plotted along both X and Y directions to determine the cluster centre. The point of maximum density obtained by fitting a Gaussian curve is considered as the centre of the cluster. The (X, Y) pixel coordinates of the cluster centre are found to be (934, 887) and (425, 500) for NGC 663 and 654, respectively. An error of a few pixels is expected in locating the cluster centre.

The cluster region is divided into a number of concentric circles to determine the radial surface density of stars. The projected radial stellar density in each concentric circle is obtained by dividing the number of stars in each annulus by its area. Densities thus obtained are plotted for different magnitude levels in the left panels of Figs 3 and 4 for the clusters NGC 663 and 654, respectively. The error bars are derived assuming that the number of stars in a concentric annulus follows the Poisson statistics.

The CO observations of this region indicate that both NGC 663 and 654 are in front of a molecular cloud (Leisawitz, Bash & Thaddeus 1989). This suggests a lack of background field stars. However, the radial density profiles shown in the left panels of Figs 3 and 4 may be affected by the presence of foreground field stars. The effect of field stars can be minimized by selecting a sample of probable MS stars lying in between the blue and red envelopes of the MS, as described by Pandey et al. (2001). To select such a sample, we defined blue and red envelopes of the MS as described in Section 7.1. The radial density distribution of the MS sample is also shown in the right panels of Figs 3 and 4 for NGC 663 and 654, respectively. The horizontal dashed line in each plot indicates the density of the blank field, as discussed in Section 2.

The radial density distribution of stars having $V < 16.0$, in the case of NGC 663, indicates that the extent of NGC 663 is about 17.5 arcmin with a core radius, defined as the radius at which the surface density drops to half of its central value, of about 3.9 arcmin. The radial density distribution of stars having $V < 19$ and $V < 20$ indicates a presence of extended corona, which is completely absent in the radial density distribution of stars with $V < 16.0$. The excess of faint stars ($V > 19$), showing almost same density distribution in both the samples, indicates an extent of the cluster up to 30 arcmin. The density of stars in the coronal region increases as we go towards the fainter end. Stars having $V \sim 19$ (i.e. $M_V \sim 4.6$) will have mass $\sim$1 $M_\odot$ and should not have reached the MS. They will lie towards the red side of the MS. Because the sample of probable MS stars also

Table 5. Comparison of the present CCD photometry with the available photometries in the literature. The difference Δ(present − literature) is in magnitude. Mean and σ are based on N stars in a V-magnitude bin.

V range	ΔV		$\Delta(B-V)$		$\Delta(U-B)$		$\Delta(V-I)$	
	Mean $\pm$ σ	N	Mean $\pm$ σ	N	Mean $\pm$ σ	N	Mean $\pm$ σ	N
NGC 663								
H61								
11.0–12.0	0.120 ± 0.256	3	−0.085 ± 0.088	3	−0.053 ± 0.009	2		
12.0–13.0	0.077 ± 0.054	2	−0.087 ± 0.087	2	−0.032 ± 0.064	2		
13.0–14.0	0.074 ± 0.036	6	−0.087 ± 0.037	6	−0.009 ± 0.060	6		
14.0–15.0	0.101 ± 0.098	2	−0.125 ± 0.053	2	−0.080 ± 0.000	1		
15.0–16.0	−0.329 ± 0.000	1	0.067 ± 0.000	1	0.021 ± 0.000	1		
PJ94								
11.0–12.0	0.025 ± 0.113	7	0.231 ± 0.408	6	0.204 ± 0.650	5		
12.0–13.0	0.070 ± 0.259	42	−0.030 ± 0.142	42	−0.009 ± 0.089	31		
13.0–14.0	−0.108 ± 0.984	52	0.004 ± 0.385	52	−0.040 ± 0.480	31		
14.0–15.0	−0.032 ± 0.544	97	0.006 ± 0.163	97	0.019 ± 0.137	72		
15.0–16.0	0.020 ± 0.299	171	0.026 ± 0.207	169	0.083 ± 0.184	118		
16.0–17.0	−0.014 ± 0.343	200	0.024 ± 0.149	197	0.101 ± 0.133	132		
17.0–18.0	−0.003 ± 0.349	201	−0.002 ± 0.153	199	0.043 ± 0.135	26		
18.0–19.0	−0.053 ± 0.238	272	−0.017 ± 0.164	264				
19.0–20.0	0.057 ± 0.277	317	−0.081 ± 0.227	180				
P01								
11.0–12.0	0.104 ± 0.124	7	−0.134 ± 0.100	6			−0.022 ± 0.242	7
12.0–13.0	0.031 ± 0.329	45	−0.058 ± 0.112	44			0.021 ± 0.179	45
13.0–14.0	0.091 ± 0.200	57	−0.014 ± 0.185	52			0.065 ± 0.111	57
14.0–15.0	0.012 ± 0.385	110	−0.008 ± 0.163	103			0.062 ± 0.070	110
15.0–16.0	0.105 ± 0.579	177	0.013 ± 0.211	153			0.062 ± 0.169	177
16.0–17.0	0.152 ± 0.404	217	0.095 ± 0.207	105			0.112 ± 0.241	217
17.0–18.0	0.189 ± 0.333	161	0.147 ± 0.218	8			0.124 ± 0.217	161
NGC 654								
JS83								
11.0–12.0	−0.035 ± 0.067	3	0.011 ± 0.043	3				
12.0–13.0	−0.135 ± 0.083	7	−0.030 ± 0.037	7				
13.0–14.0	−0.098 ± 0.097	11	−0.026 ± 0.087	11				
14.0–15.0	−0.037 ± 0.131	11	0.012 ± 0.112	11				
15.0–16.0	0.413 ± 0.356	2	−0.406 ± 0.460	2				
PJ94								
11.0–12.0	−0.055 ± 0.050	3	0.037 ± 0.048	3				
12.0–13.0	−0.031 ± 0.037	10	−0.018 ± 0.029	10				
13.0–14.0	−0.071 ± 0.069	15	0.001 ± 0.057	15				
14.0–15.0	−0.123 ± 0.356	30	−0.015 ± 0.094	29				
15.0–16.0	−0.034 ± 0.070	45	−0.023 ± 0.089	44				
16.0–17.0	−0.055 ± 0.223	63	−0.049 ± 0.119	63				
17.0–18.0	−0.035 ± 0.097	81	−0.002 ± 0.180	76				
18.0–19.0	−0.001 ± 0.094	116	−0.061 ± 0.140	109				
19.0–20.0	−0.015 ± 0.093	99	−0.089 ± 0.213	95				
20.0–21.0	−0.073 ± 0.151	41	−0.043 ± 0.259	22				

shows an excess of faint stars, it poses an interesting question for the age spread in the cluster. Although the width of the MS strip is ∼0.8 in (V–I) colour (see Fig. 13) it seems unlikely that the sample of stars having $V < 19.0$ is mainly comprised of pre-main-sequence (PMS) stars.

For the cluster NGC 654, Fig. 4 indicates almost the same radial distribution for different magnitudes bin levels. The density distribution of stars does not show any excess of low-mass stars in the outer region, as in the case of NGC 663.

To parametrize the radial density profiles at different limiting magnitude levels, we follow the approach by Kaluzny & Udalski (1992). Because of low S/N ratio in the star counts of open clusters, it is not an easy task to constrain the tidal radius of cluster using the empirical model of King (1962). We describe radial density $\rho(R)$ as

$$\rho(R) \propto \frac{f_{\rm o}}{1 + (r/r_{\rm c})^2},$$

where $r_{\rm c}$ is the core radius (the radius at which the surface density falls to half of the central density $f_{\rm o}$). In the case of NGC 663, we fit the above function to the observed radial density profile of stars having $V < 16$. The fit was performed for the data that lie within radii 17.5 and 30 arcmin. These two limits were selected because the first (i.e. $r = 17.5$ arcmin) represents cluster extent for brighter stars, whereas the other value of radius (30 arcmin) represents the extent of distribution of faint coronal stars ($V \geqslant 19$). Both data sets

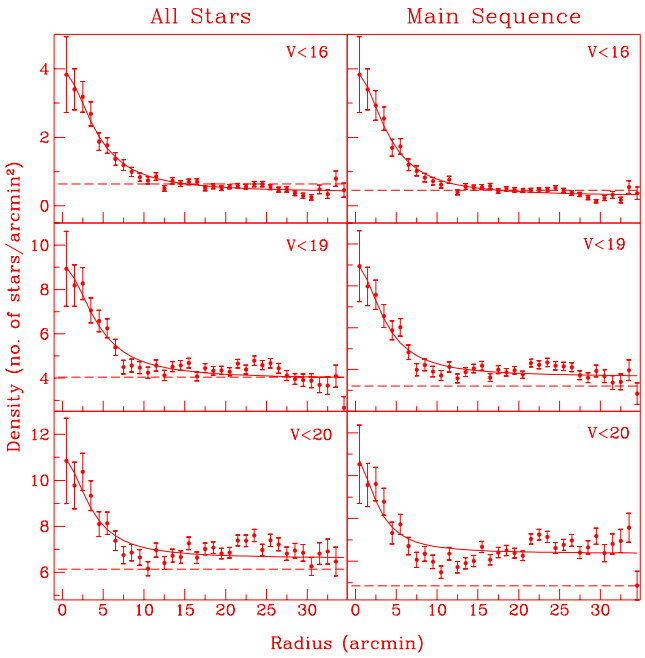

Figure 3. The radial variation of the projected stellar density of NGC 663 for different magnitude levels. Dashed lines show the density of field stars.

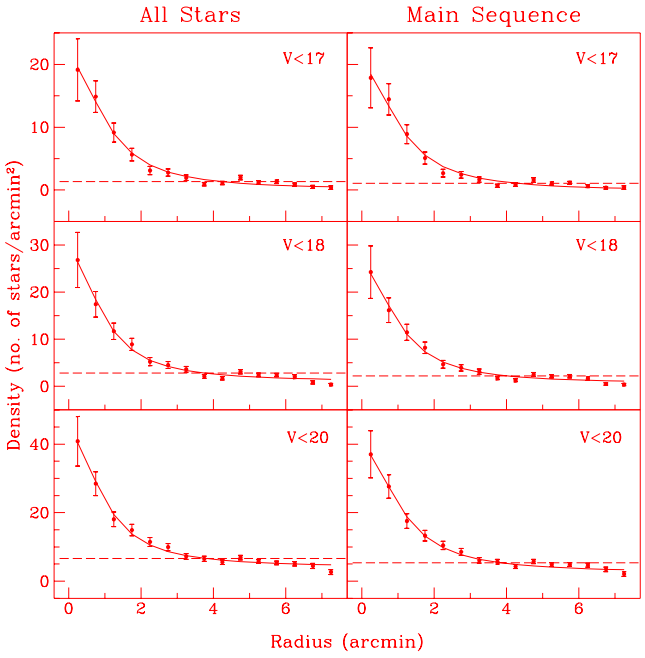

Figure 4. Same as Fig. 3, but for NGC 654.

give identical radial density profile with $r_c \sim 3.9$ arcmin. The value of core radius obtained in the present work is in agreement with that obtained by Nilakshi et al. ($r_c = 3.75$ arcmin) using the DSS. Because the radial density distribution of stars having $V > 19/20$ shows an excess of stars in the coronal region of the cluster ($r > 17.5$ arcmin), we performed the fit for the data having $r \leqslant 17.5$ arcmin. The best fit obtained by the χ^2 minimization technique is shown in Fig. 3. The value of r_c is found to be $\sim 4.2 \pm 0.5$ arcmin. This indicates that core size of the cluster NGC 663 does not change for the distribution of faint (i.e. low-mass) stars.

For the cluster NGC 663, PJ94 estimated the outer radius $R_{full} = 4.4$ arcmin with $R_{HWHM} = 2.7$ arcmin, which are significantly smaller than the values obtained in the present work.

To study the cluster properties in detail we divided the cluster NGC 663 into three subregions as the core ($r \leqslant 4.2$ arcmin) and outer region ($4.2 < r \leqslant 17.5$ arcmin). A subsample of the data having $r \leqslant 10$ arcmin was also studied to compare our results with those obtained by PJ94.

The function (equation 1) was fitted to the observed radial density profile of NGC 654. The best fit obtained by the χ^2 minimization technique is shown in Fig. 4. The value of core radius r_c is found to be 0.9 ± 0.1 arcmin and the extent of the cluster NGC 654 is estimated to $\sim$3.7 arcmin. For the cluster NGC 654, PJ94 have obtained $R_{full} = 3.3$ arcmin and $R_{HWHM} = 1.4$ arcmin, which are comparable to the values obtained in the present work. However, Stone (1980) obtained the extent of the core and corona of the cluster as 4 and 16 arcmin, respectively, which are significantly larger than the values obtained in the present work and in PJ94. The core radius obtained by Nilakshi et al. (2002) is in good agreement with that obtained here, whereas the cluster extent obtained by them ($\sim$10 arcmin) is greater than the value obtained in the present work. The cluster properties are studied in detail in two subregions having $r \leqslant 0.9$ arcmin (core) and $0.9 < r \leqslant 3.7$ arcmin (outer region).

6 INTERSTELLAR EXTINCTION

6.1 Reddening

The CO observations of this region indicate that the clusters NGC 663 and 654 are in front of a molecular cloud (see Leisawitz et al. 1989; PJ94). In the literature, the reported values of $E(B–V)$ range from 0.70 to 1.00 mag (Leisawitz et al. 1989; PJ94; P01) and 0.70 to 1.20 mag (PJ94) for the clusters NGC 663 and 654, respectively.

The $(U–B)/(B–V)$ two-colour diagram (TCD), for the three subregions of NGC 663 mentioned in Section 5, is shown in Fig. 5, where we plot the data only for those stars which have $V_{error} \leqslant 0.05$. This figure is used to estimate the reddening $E(B–V)$ in the three regions. In Fig. 5, an unreddened MS for $z = 0.02$ by Bertelli et al. (1994) is shifted along a normal reddening vector [i.e. $E(U–B)/E(B–V) = 0.72$] to match the observations and a mean reddening of $E(B–V) \sim 0.75$ is estimated in the cluster region. In the cluster region, reddening $E(B–V)$ varies from 0.62 to 0.95, indicating a variable reddening in the cluster region. This indicates that the cluster has emerged from its parent clouds in the recent past.

The reddening in the cluster NGC 654 varies from $E(B–V)_{min} \sim 0.75$ mag to $E(B–V)_{max} \sim 1.15$ mag (JS83; PJ94). In the case of NGC 654, Samson (1975) claimed that the stars within the radius $\sim$3 arcmin were less reddened than those located outside this radius. Huestamendia et al. (1993) confirmed the trend found by Samson (1975).

6.2 Spatial variation of reddening

The spatial distribution of interstellar matter within the clusters can be studied with the help of the $(U–B)/(B–V)$ TCD. Fig. 5 indicates a variable reddening in the NGC 663 region. Reddening $E(B–V)$ varies in the inner region from 0.65 to 0.85 mag, whereas in the outer regions the reddening varies from 0.62 to 0.95 mag. Thus, the differential reddening $\Delta E(B–V) = E(B–V)_{max} - E(B–V)_{min}$ varies from 0.20 mag in the inner region to 0.33 mag in the outer region.

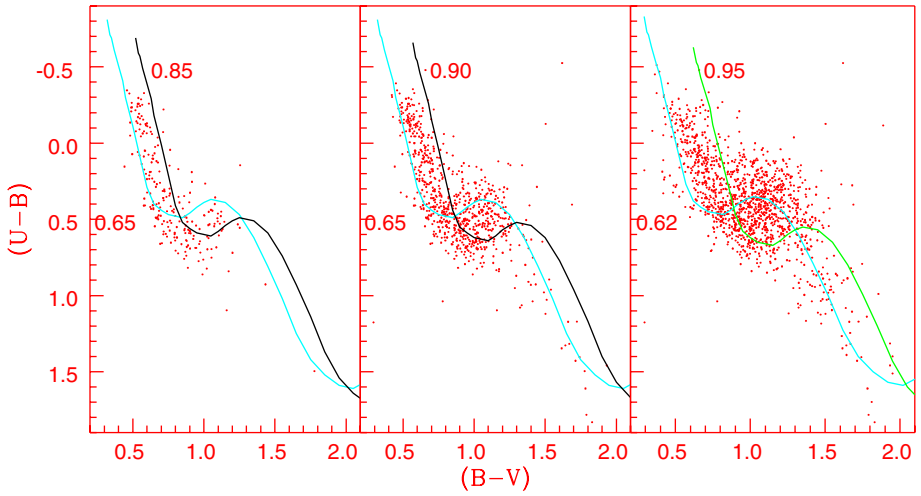

Figure 5. $(U–B)/(B–V)$ TCD for the stars in three subregions of the cluster NGC 663. The continuous curve represents the MS shifted along a normal reddening vector for the $E(B–V)$ value mentioned along the curve.

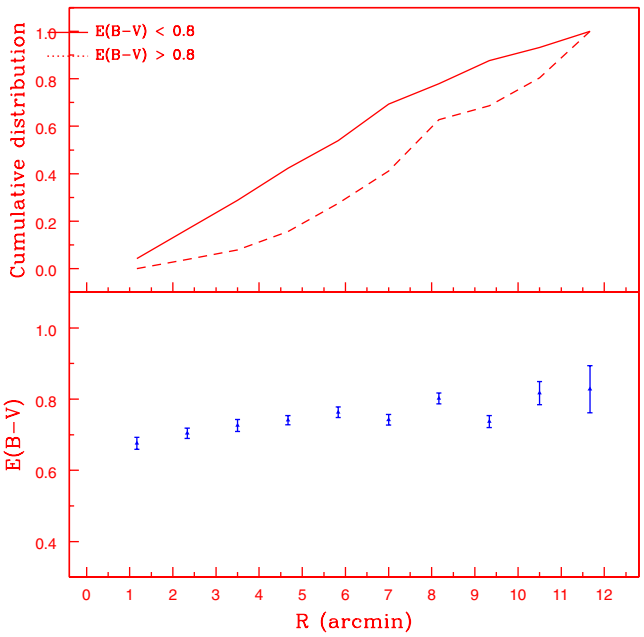

Figure 6. The radial variation of the reddening $E(B–V)$ (lower panel) and the cumulative distribution of two subgroups of stars (upper panel) in the NGC 663 cluster region. The error bars represent standard errors.

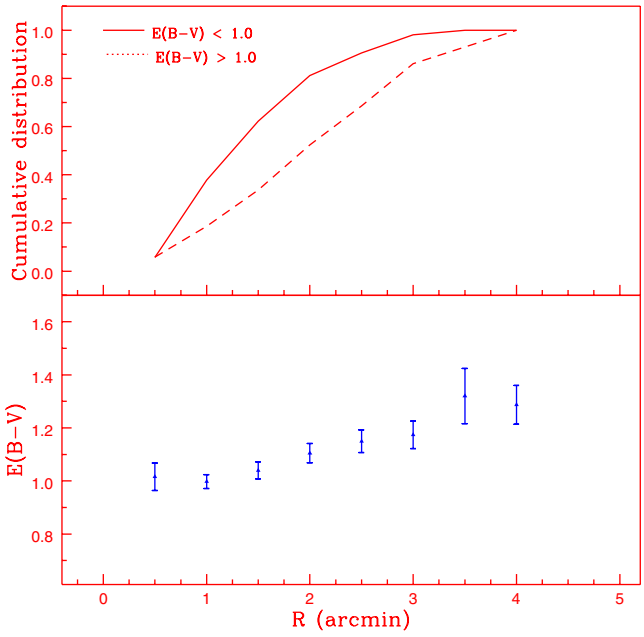

Figure 7. Same as Fig. 6, but for NGC 654.

The reddening for individual stars ($V_{\rm error} \leqslant 0.05$), having spectral type earlier than A0, has been derived using the Q-method (Johnson & Morgan 1953). Because we do not have U-band observations for NGC 654, we used the U-band observations given by PJ94. The distribution of reddening as a function of radial distance is shown in lower panel of Figs 6 and 7 for NGC 663 and 654, respectively, which indicates a deficiency of reddening material in the central region of both clusters.

We divided the sample of NGC 663 into two groups: one for stars having $E(B–V) < 0.80$ and the other having $E(B–V) \geqslant 0.80$. Similarly, two subgroups, $E(B–V) < 1.0$ and $E(B–V) > 1.0$, were made for the cluster NGC 654. The cumulative distribution of these subsamples as a function of radial distance is plotted in upper panel of Figs 6 and 7 for the clusters NGC 663 and 654, respectively. A Kolmogorov–Smirnov test confirms the trend in both clusters at a confidence level better than 99 per cent that the stars close to the centre are less reddened than those located in the coronal region of the cluster.

6.3 Reddening law

6.3.1 NGC 663

Using the colour excess $E(V–K)$ and $E(B–V)$, Tapia et al. (1991) have found weak evidence for an anomalous reddening law with a value of $R_{\rm cluster}$ (total to selective extinction in the cluster region) = 2.73 ± 0.20, which is marginally lower than the normal value of 3.1, although the scatter in their data is too large to conclude about the value of $R_{\rm cluster}$. Yadav & Sagar (2001) reported values for $E(\lambda–V)/E(B–V)$, which are significantly smaller than the normal ones.

In a detailed analysis (Pandey et al. 2003) using the $E(\lambda-V)/E(B-V)$ and $(\lambda-V)/(B-V)$ diagrams, we have studied the reddening law in the NGC 663 cluster region and found a marginally higher than normal value for $R_{\rm cluster}$ (=3.38 ± 0.34). We have also found that the $V/(U-B)$ colour–magnitude diagram (CMD) does not support a normal value for the reddening vector $X = 0.72$. Because the error in the estimation of $R_{\rm cluster}$ is quite large, we prefer a normal value of $R_{\rm cluster}$ in the NGC 663 region for further analysis.

6.3.2 NGC 654

Using the variable extinction analysis, Turner (1976) and Stone (1980) found values of $R_{\rm cluster}$ of (2.9 ± 0.2) and (2.9 ± 0.6), respectively. Sagar & Yu (1989) concluded that at wavelengths greater than 5500 Å, the extinction is normal. The presence of unusually well-aligned interstellar grains indicated by the polarization measurements seems to increase the extinction in U and B slightly. Sagar & Yu (1989) found a colour-excess ratio $E(V-K)/E(B-V) = 2.53 \pm 0.28$, which yields $R_{\rm cluster}$ [$1.1 \times E(V-K)/E(B-V) = 2.78 \pm 0.31$]. In a recent work, Pandey et al. (2003) found a value of $R_{\rm cluster}$ (2.98 ± 0.15), which, within the error, is close to the normal value of 3.1. Most of the reported values indicate a lower value of $R_{\rm cluster}$ in the NGC 654 region, although the reported errors are quite large to conclude the reddening law in this region.

The dust causing the reddening is also a source of polarization. Interstellar polarization has long been attributed to the partial alignment of non-spherical grains by the galactic magnetic field (Davis & Greenstein 1951). Observations of polarization give information on both the size and the composition of the grains. Serkowski, Mathewson & Ford (1975) have shown that the wavelength of maximum linear polarization, $\lambda_{\rm max}$, is a characteristic grain size parameter. As the value of $\lambda_{\rm max}$ is expected to vary with mean grain radius, a correlation with the ratio of total-to-selective extinction, $R = A_V/E(B-V)$, is implied. Serkowski et al. (1975) obtained a dependence of $\lambda_{\rm max}$ on R as $R = 5.5\lambda_{\rm max}$ ($\lambda_{\rm max}$ in μm). Whittet & van Breda (1978) further refined the dependence as $R = (5.6 \pm 0.3)\lambda_{\rm max}$.

Photographic polarimetric measurements of NGC 654 were first made by Samson (1976), who found the cluster stars to be polarized parallel to the galactic plane. To study the behaviour of dust grains and extinction law in the cluster region, we have carried out multiwavelength polarimetric observations of seven stars in the *BVRI* bands ($\lambda_{B_{\rm eff}} = 0.44$ μm, $\lambda_{V_{\rm eff}} = 0.53$ μm, $\lambda_{R_{\rm eff}} = 0.70$ μm, $\lambda_{I_{\rm eff}} = 0.83$ μm). The observations were carried out between 1992 October and 1993 January, with a fast star and sky chopping polarimeter (Jain & Srinivasulu 1991) at the Cassegrain focus of the 1.02-m telescope at the Vainu Bappu Observatory (VBO), Kavalur, of the Indian Institute of Astrophysics. The instrumental polarization was determined by observing unpolarized reference stars from Serkowski (1974) and its average was found to be ∼0.1 per cent. It was subtracted vectorally from the measured polarization of the programme stars. The zero of the polarization position angle was determined by observing the polarized standard stars (Hsu & Berger 1982).

Table 7 lists the percentage of polarization (P_λ), the position angle of the electric vector (θ_λ) in the equatorial coordinate system and their respective mean errors for each filter. Star identifications are taken from JS83. The membership determination was made on the basis of JS83 and Sagar & Yu (1989), and these are indicated in Table 7. Non-member stars 57 and 137 both have relatively lower values of polarization ($P_V \sim 2$ per cent). Star 161 also shows a similarly low polarization ($P_V \sim 2$ per cent). Its cluster membership probability is also low (48 per cent). It is also characterized by a relatively low value of reddening [$E(B-V) = 0.28$]. This star is likely to be a non-member star in the foreground. The cluster-member stars (9, 68, 109, 111) show relatively larger polarization (>3 per cent). The polarization position angle is nearly the same ($\theta_V \simeq 94^\circ$) for all the member stars, while the percentage polarization shows considerable variation (P_V ranges from 3.03 to 4.47 per cent). This differential polarization may be related to the differential extinction across the cluster. It is also to be noted that the mean polarization position angle ($\theta_V \simeq 94^\circ$) for the cluster-member stars is systematically different from the mean position angle ($\theta_V \simeq 104^\circ$) for the non-members. These position angles may be representative of the magnetic field directions in the spiral arms in the galactic disc, the non-cluster member stars being polarized by the interstellar

Table 6. CF of photometric data in the clusters NGC 663 and 654, and the field region.

V range	NGC 663	NGC 654	Field region
13–14	1.00	1.00	100
14–15	0.99	1.00	100
15–16	0.98	1.00	100
16–17	0.95	1.00	100
17–18	0.91	0.99	0.99
18–19	0.84	0.97	0.97
19–20	0.68	0.96	0.96

Table 7. Polarimetric observations of stars in NGC 654.

Star	*V* mag	Membership probability (per cent)	Filter	P_λ	θ_λ
9	9.33	92	*B*	2.00 ± 0.47	98 ± 7
			V	3.03 ± 0.16	92 ± 2
			R	2.68 ± 0.11	94 ± 1
			I	2.31 ± 0.17	98 ± 2
57[a]	9.47	90	*B*	2.16 ± 0.36	97 ± 5
			V	2.03 ± 0.15	102 ± 2
			R	1.48 ± 0.14	98 ± 3
			I	1.25 ± 0.26	97 ± 6
68	9.56	84	*B*	4.18 ± 0.70	85 ± 5
			V	4.47 ± 0.19	95 ± 1
			R	3.78 ± 0.11	94 ± 1
			I	3.42 ± 0.18	95 ± 2
109	10.62	90	*B*	3.86 ± 0.22	92 ± 2
			V	3.82 ± 0.06	96 ± 1
			R	3.23 ± 0.05	96 ± 1
			I	3.00 ± 0.07	95 ± 1
111	7.32	86	*B*	3.37 ± 0.26	93 ± 2
			V	3.76 ± 0.09	93 ± 1
			R	3.32 ± 0.06	93 ± 1
			I	2.78 ± 0.08	93 ± 1
137[a]	10.86	0	*V*	2.53 ± 0.32	106 ± 4
			R	2.03 ± 0.18	114 ± 3
			I	1.51 ± 0.29	111 ± 6
161	9.87	48	*V*	2.00 ± 0.21	104 ± 3
			R	1.94 ± 0.17	110 ± 2
			I	1.81 ± 0.29	103 ± 5

[a]Non-members (see Sagar & Yu 1989).

Table 8. Polarization results in NGC 654.

Star[a] no.	P_{max} per cent	λ_{max} (μm)	$E(B–V)^{a,b}$ (mag)	$E(V–K)^{a}$ (mag)
9	2.94 ± 0.30	0.53 ± 0.05	0.75	2.26
57[c]	2.23 ± 0.16	0.39 ± 0.02	0.31	0.78
68	4.36 ± 0.30	0.50 ± 0.03	0.93	–
109	3.77 ± 0.27	0.50 ± 0.03	1.05	2.29
111	3.73 ± 0.10	0.50 ± 0.02	0.93	2.33
137[c]	2.76 ± 0.10	0.41 ± 0.01	1.26	–
161	2.02 ± 0.07	0.59 ± 0.02	0.28	0.64

[a]Sagar & Yu (1989). [b]JS83. [c]Non-member.

dust in the local Orion arm, and the cluster-member stars being polarized by dust primarily in the Perseus arm about 2 kpc away.

From the observation of amount polarization in several passbands, we can compute the wavelength at which maximum polarization occurs. This wavelength λ_{max} is a function of the optical properties and characteristic particle size distribution of aligned grains (McMillan 1978). λ_{max} (in μm) at which P_{max} (in per cent) occurs have been calculated by fitting the observed polarization in the *BVRI* bands to the standard Serkowski polarization law

$$P_\lambda / P_{max} = \exp[-k \ln^2(\lambda_{max}/\lambda)],$$

and adopting $k = 1.15$. Table 8 lists P_{max} and λ_{max} for seven stars. Colour excess $E(B–V)$ and $E(V–K)$ values have been taken from Sagar & Yu (1989). The mean λ_{max} value for member stars is found to be 0.50 ± 0.03, which is smaller than the usual value (0.545 ± 0.04 μm). As λ_{max} is proportional to grain radius (Greenberg 1968), λ_{max} indicates that the grains associated with NGC 654 are smaller than those in the general interstellar medium.

It is well known (Hiltner 1956) that for the diffuse interstellar medium the polarization efficiency (ratio of the maximum amount of polarization to visual extinction) cannot exceed the empirical limit

$$P_{max} \leqslant 3A_V \simeq 3R\,E(B–V).$$

The ratio $P_{max}/E(B–V)$ depends mainly on the alignment efficiency, the magnetic field strength and the amount of depolarization due to the radiation traversing more than one cloud with different field directions. As can be seen in Fig. 8, where P_{max} values for the observed stars are plotted as a function of $E(B–V)$, none of the stars lies to the left of the interstellar maximum line. This situation indicates that the observed polarization is most likely due to the diffuse interstellar material. In the lower part of the plot, non-members stars 57 and 161 lie close to the limiting line, indicating a maximum polarization efficiency. The observations of the stars of NGC 654 in Fig. 8 are well bounded by the line $P_{max}/E(B–V) \sim 5$ per cent mag^{-1} drawn in the figure as a dotted line. This indicates a relatively low polarization efficiency. The mean polarization of member stars of NGC 654 is found to be $\overline{P}_{max} = 3.73 \pm 0.17$ per cent, whereas mean polarization for field stars is estimated as 2.26 ± 0.09 per cent. Fosalba et al. (2002) have studied the galactic interstellar polarization and found that polarization degree P per cent depends on the galactic longitude and can be represented by the following relation: P per cent $\simeq 1.3 \pm 0.9 \sin(2l + 180^\circ)$. For the position of NGC 654 ($l = 129\overset{\circ}{.}09$), the polarization degree is found to be ∼2.2 per cent, which is in good agreement with the value (2.26 ± 0.09 per cent) obtained in the present work for the field stars towards the direction of NGC 654.

The parameters λ_{max} and R_V are related to the mean size of the particles responsible for polarization and extinction, respectively, at visible wavelengths. If the extinction is dominated by aligned

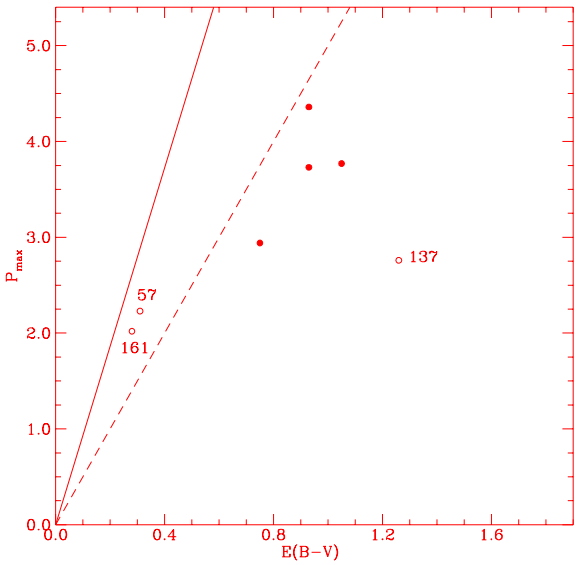

Figure 8. Polarization efficiency diagram for stars in the NGC 654 cluster region. Member stars shown by filled circles. The solid line represents optimum efficiency (9.3 per cent mag^{-1}) in the general interstellar medium assuming $R_V = 3.1$. The dashed line represents an efficiency of ∼5 per cent mag^{-1}.

component of grains whose size distribution is correlated with the environment that of the polarizing grains, then λ_{max} and R_V or $E(V–K)/E(B–V)$ are correlated. In Fig. 9 we plot λ_{max} as a function of $E(V–K)/E(B–V)$ for five stars. The dashed lines display the boundaries of the distribution of stars given by (Whittet & van Breda 1978, see their fig. 1). The member stars of NGC 654 are well inside the boundaries of the distribution by Whittet & van Breda (1978), whereas the non-members do not follow the relation. This indicates that the grains in NGC 654 that produce optical polarization contribute significantly to the optical extinction. Whittet & van Breda (1978) deduced that the ratio of total-to-selective extinction R_V and the wavelength of maximum polarization λ_{max} are correlated by the

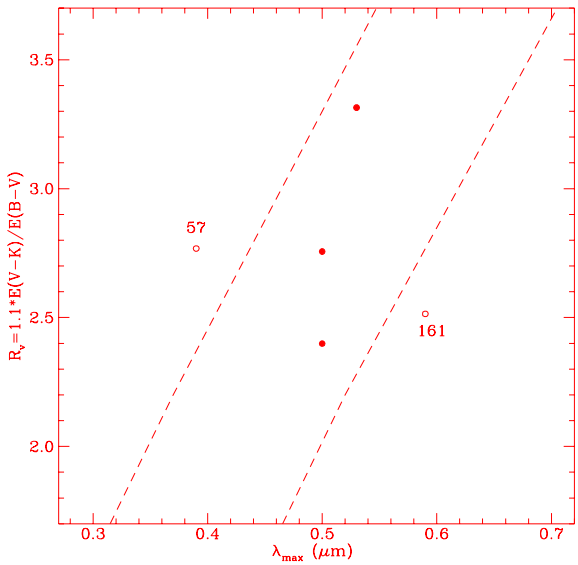

Figure 9. Plot of λ_{max} versus R_V for five stars in the NGC 654 region. Member stars are shown by filled circles. The dashed lines represent the boundaries of the distribution of stars given by Whittet & van Breda (1978).

equation $R_V = (5.6 \pm 0.03)\lambda_{max}$. Following the above relation, R_V for the cluster is found to be 2.80 ± 0.15. The colour-excess ratio by Sagar & Yu (1989) gives $E(V-K)/E(B-V) = 2.53 \pm 0.28$. Following the relation $R_V = 1.1\ E(V-K)/E(B-V)$ (Whittet & van Breda 1978), the value of R_V for NGC 654 region is found to be 2.78 ± 0.31. Pandey et al. (2003) have found a value of 2.97 ± 0.30 for R_V in the NGC 654 region. The value of mean λ_{max} (0.50 ± 0.03), and consequently the value of R_V obtained in the present work and those obtained by Sagar & Yu (1989) and Pandey et al. (2003), indicate that the dust grains associated with NGC 654 are smaller than those associated with the general interstellar medium.

7 COLOUR–MAGNITUDE DIAGRAMS

7.1 NGC 663

The stars in the NGC 663 region show a well-defined but broad MS in the CMDs, displayed in Fig. 10. The effect of foreground field stars is seen as we move towards the outer region. The absence of background stars (i.e. blueward of the MS) supports the CO observations that NGC 663 is located in front of a molecular cloud. As we have discussed earlier (see Section 4), the fact that the cluster region shows a variable reddening, apart from the photometric errors, presence of field stars and binaries should be a main cause of broadening of the MS.

7.2 NGC 654

Fig. 11 shows a well-defined MS in the CMDs of two subregions of NGC 654 as defined in Section 5. The presence of foreground field stars is clearly visible in the outer region of the cluster. There are no background field stars seen in the CMDs, which indicates that the cluster NGC 654 may be located in front of a molecular cloud. This conclusion is consistent with radio observations by Leisawitz et al. (1989).

7.3 Blank field

The V, $(V-I)$ CMD for the blank field covering an area of $\sim 6 \times 6$ arcmin^2 is shown in Fig. 12, which indicates that the CMDs of NGC 663 and 654 cluster regions have significant contamination towards the fainter end due to field stars.

7.4 Cluster membership

To study the LF/MF, it is necessary to remove field star contamination from the sample of stars in the cluster region. Membership determination is also crucial for assessing the presence of PMS stars, because PMS stars and dwarf foreground stars both occupy similar positions above the zero-age main sequence (ZAMS) in the CMD. In the absence of a proper motion study, we used the statistical criterion to estimate the number of stars in the cluster region. The contamination due to field stars is greatly reduced if we select

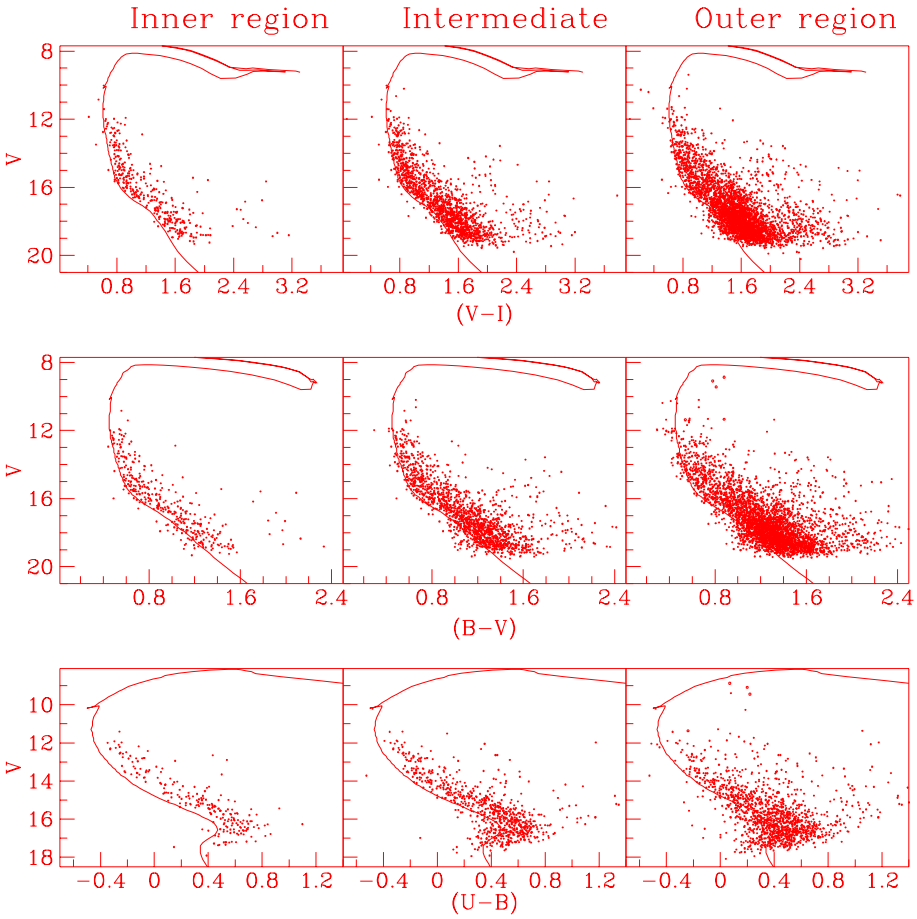

Figure 10. The CMDs in the three subregions of the cluster NGC 663. The isochrone by Bertelli et al. (1994) for solar metallicity and log age = 7.4 is also shown.

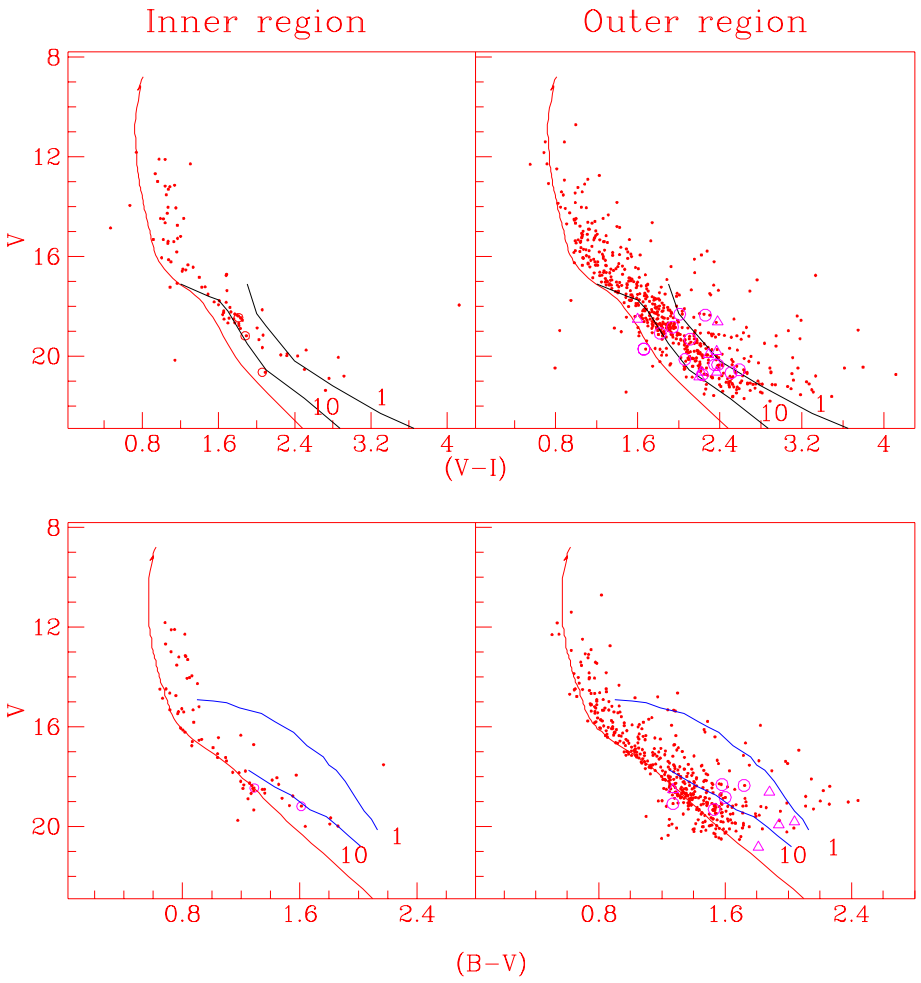

Figure 11. The CMDs in the two subregions of the cluster NGC 654. The isochrone for log age = 7.0 and PMS isochrones for 1 and 10 Myr are also shown.

a sample of stars which are located near the well-defined MS. We define blue and red envelopes for the MS on the $V/(V–I)$ CMD for stars lying within the cluster boundary, and these are shown in Fig. 13 for both the clusters. The same envelopes were used for the blank field region $V/(V–I)$ CMD to estimate contamination in the cluster region due to the presence of field stars. After normalizing the area, we can find the number of field stars present per unit area in each magnitude bin. The number of probable cluster members in the subregions of the cluster was obtained by subtracting the contribution of field stars (corrected for data incompleteness) from each magnitude bin of the contaminated sample of MS stars (also corrected for data incompleteness). The statistics is given in Table 9. As expected, field star contamination increases from the inner region to the outer region.

7.5 Age and distance

7.5.1 NGC 663

Because most of the bright stars are saturated even on our short-exposure frames, we are unable to derive from our observations the turn-off age for the cluster. Using the photoelectric photometry by H61 for bright stars, PJ94 reported an age spread of ∼13–15 Myr in star formation, with some stars having been formed as recently as ∼10–12 Myr ago. Data compiled by Leisawitz (1988) give a median age of ∼20 Myr for NGC 663. Recently, P01 have also reported the age of the cluster in the range 20–25 Myr. We have overplotted an isochrone for $Z = 0.02$ and log age = 7.4 by Bertelli et al. (1994) for $E(B–V)_{\rm min} = 0.65$ in Fig. 10 and found a distance modulus $(m - M_V) = 14.40 \pm 0.10$. While fitting the isochrones, the colour-excess ratio $E(U–B)/E(B–V) = 0.60$ was used (for details, see Pandey et al. 2003), whereas a normal value of $E(V–I)/E(B–V) = 1.25$ was used.

In Fig. 14 we have plotted the dereddened CMD for the cluster stars in the region having $r \leqslant 4.2$ arcmin to reduce the contamination due to field stars. The dereddened magnitude $V_{\rm o} = (V - A_V)$ has been obtained for a normal extinction law (i.e. $R = 3.1$). The data for bright stars have been taken from H61. Post-main-sequence stars indicate an age spread in star formation of ∼10–15 Myr with a mean age ∼13 Myr. It is interesting to mention that the statistics about probable MS cluster members given in Table 9 indicates that ∼1-$M_\odot$ stars are on the MS. The time required by ∼1 $M_\odot$ to reach the MS is ∼50 Myr. If the statistics is true, the cluster NGC 663 may have even larger age spread with low stars formed much earlier.

The apparent distance modulus $(m - M_V) = 14.40 \pm 0.10$ and $E(B–V)_{\rm mean} = 0.80$, for a normal reddening law (i.e. $R_V = 3.1$), corresponds to a distance of 2.42 ± 0.12 kpc. The age and distance obtained in the present work are in good agreement with those reported in previous studies.

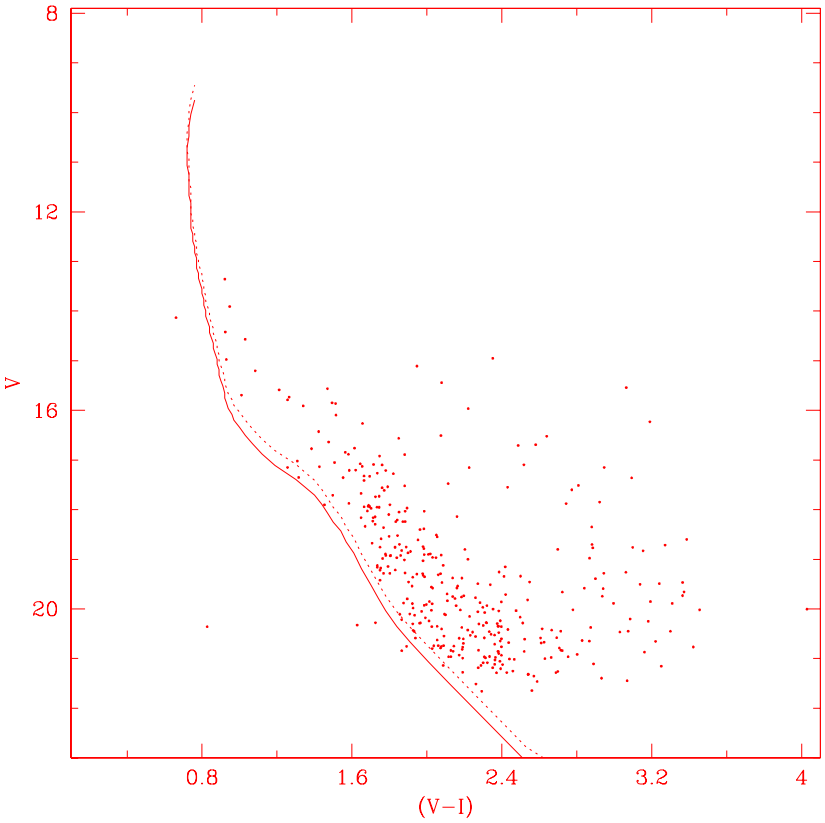

Figure 12. The V, $(V–I)$ CMD of the blank field region. The isochrone for log age = 7.0, shifted for $(m - M) = 14.7$ mag (solid curve) and 14.4 mag (dashed curve) is also shown.

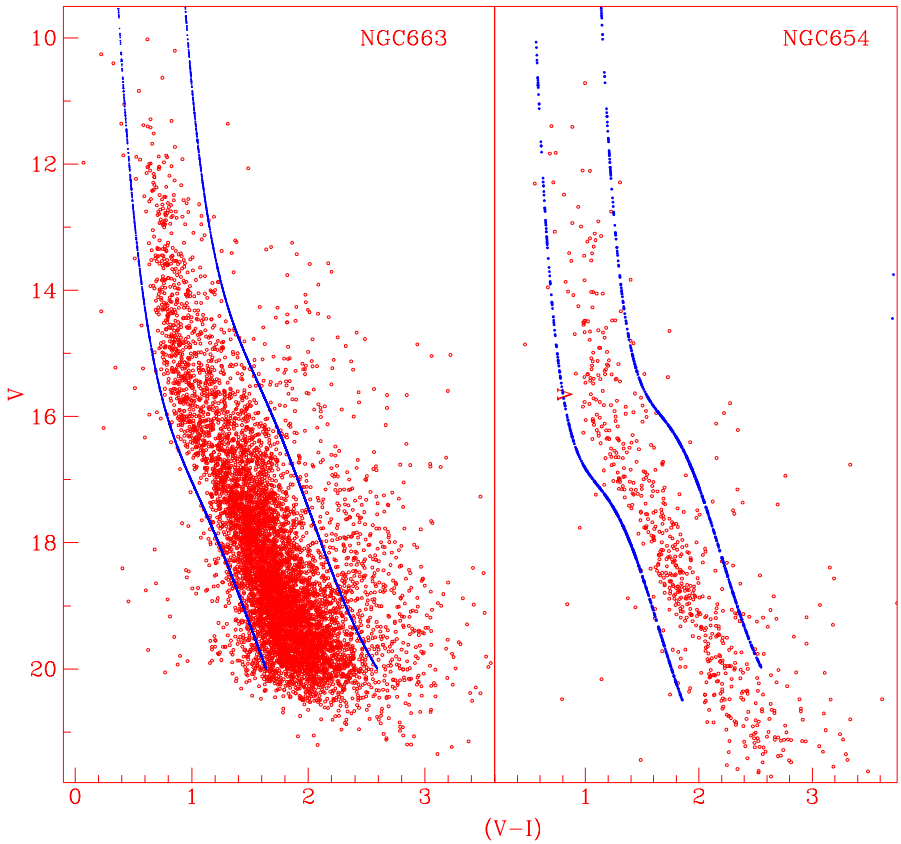

Figure 13. The V, $(V–I)$ CMD for stars lying within the cluster boundary with blue and red envelopes delimiting the MS stars (see text).

Table 9. LF for the subregions of clusters NGC 663 and 654. n_c and n_f are the number of stars (corrected for the data incompleteness) in the subregions of the clusters and the number of expected field stars, respectively, and n_p is number of probable cluster member. The intermediate region, in the case of NGC 663, also includes the inner region (see text).

Cluster	Range	Inner region			Intermediate region			Outer region			Whole region		
	V mag	n_c	n_f	n_p	n_c	n_f	n_p	n_c	n_f	n_p	n_c	n_f	n_p
NGC 663	10–11	2.0	0.0	2.0	3.0	0.0	3.0	2.0	0.0	2.0	4.0	0.0	4.0
	11–12	4.0	0.0	4.0	8.0	0.0	8.0	13.0	0.0	13.0	17.0	0.0	17.0
	12–13	22.0	0.0	22.0	42.0	0.0	42.0	49.0	0.0	49.0	71.0	0.0	71.0
	13–14	24.0	3.1	20.9	60.0	17.4	42.6	84.0	50.3	33.7	108.0	53.5	54.5
	14–15	37.4	4.7	32.7	104.0	26.2	77.8	189.9	75.4	114.5	227.3	80.2	147.1
	15–16	66.3	14.2	52.1	183.0	78.5	104.5	327.6	226.3	101.3	393.9	240.5	153.4
	16–17	76.8	17.3	59.5	246.0	78.5	167.5	603.2	276.6	326.6	680.0	294.0	386.0
	17–18	84.6	60.4	24.1	393.0	322.7	70.9	1094.5	965.6	128.9	1179.0	1026.2	152.9
	18–19	117.9	79.6	38.3	514.0	436.1	77.9	1747.6	1269.9	477.7	1865.5	1349.5	516.0
	19–20	142.6	93.6	49.0	796.0	505.9	290.1	2720.6	1493.7	1226.9	2863.2	1587.4	1275.8
NGC 654	11–12	1.0	0.0	1.0				3.0	0.0	3.0	4.0	0.0	4.0
	12–13	4.0	0.0	4.0				5.0	0.0	5.0	9.0	0.0	9.0
	13–14	6.0	0.1	5.9				9.0	2.3	6.7	15.0	2.4	12.6
	14–15	8.0	0.3	7.7				21.0	4.6	16.4	29.0	4.9	24.1
	15–16	8.0	0.6	7.4				41.0	10.4	30.6	49.0	11.0	38.0
	16–17	11.0	0.7	10.3				56.0	12.8	43.2	67.0	13.5	53.5
	17–18	8.1	2.5	5.6				79.1	43.4	35.7	87.2	45.9	41.3
	18–19	21.7	3.4	18.3				105.5	58.6	46.9	127.2	61.9	65.3

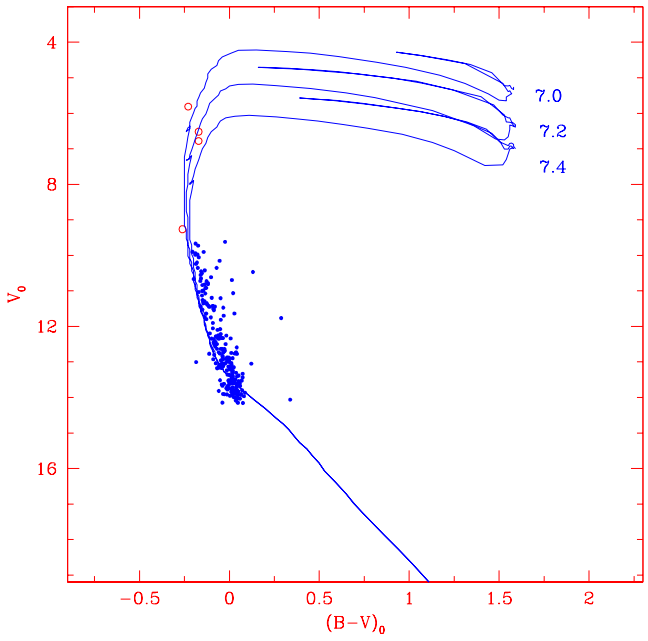

Figure 14. The dereddened V_o, $(B–V)_o$ CMD for the stars within the cluster region ($r \leqslant 4.2$ arcmin) of NGC 663. The isochrones for solar metallicity by Bertelli et al. (1994) for various ages have also been plotted. The data for bright stars have been taken from H61 (open circles). A correction of $\Delta = 0.1$ and $\Delta(B–V) = -0.09$ was applied to H61 data (see Table 5).

7.5.2 NGC 654

The bright stars could not be observed also in the case of NGC 654. Supplementing their CCD data with the photoelectric observation of bright stars by JS83, PJ94 reported a time spread of star formation in NGC 654 of at least ∼20 Myr with a mean age of about 15 Myr. Star formation time may be longer if another star having membership probability of 0.92 is considered. The compilation of Leisawitz (1988) gives an age ranging between 15 and 40 Myr.

An isochrone of log age = 7.0 having solar metallicity is overplotted on the CMDs shown in Fig. 11. We find a good fit for the blue envelope of the MS for $E(B–V)_{min} = 0.82$ and distance modulus $(m - M) = 14.7 \pm 0.1$. A normal value for colour-excess ratio $E(V–I)/E(B–V) = 1.25$ was used. The CMDs indicate that stars having $V \sim 17.0$ mag ($M_V \sim 2.3$, mass ∼1.7 $M_\odot$) have already reached the MS, whereas stars having $V > 17.0$ mag can be seen on the PMS. The statistics of stars, having $V \geqslant 18.0$, in the cluster as well as field region, is shown in Fig. 15, which manifests a significant number of cluster members on the PMS stage. Here, it is interesting to mention that the stars brighter than $V \sim 15$ in the central region are away from the isochrones, whereas in the outer region the brighter stars nicely follow the isochrone of 10 Myr. Keeping in mind that the stars in the central region are less reddened (Section 6.2), Fig. 11 indicates that the stars in the central region are older than those in the outer region.

The spectra of PMS stars often show emission in the Balmer lines, particularly in Hα. The PMS stars in the young open clusters can be detected using the $(R–H\alpha)/(V–I)$ and $V/(R–H\alpha)$ diagrams as suggested by Sung, Bessel & Lee (1998). We have carried out Hα photometry of NGC 654, and the $V/(R–H\alpha)$ and $(R–H\alpha)/(V–I)$ diagrams are shown in Figs 16 and 17, respectively. Those stars that we identify as having Hα emission and may be PMS stars are shown by filled circles and are listed in Table 10. The solid line in Fig. 17 represents the reddened [applying $E(V–I)_{mean} = 1.13$] MS relation for NGC 2264 (Sung et al. 1998). Assuming no reddening effect on the $(R–H\alpha)$ colour, we adjusted the curve for $(R–H\alpha)$ visually because our Hα magnitudes are not calibrated. The probable PMS stars are marked as open circles and open triangles in the CMDs shown in Fig. 11. The stars shown by open triangles are located outside the boundary of the cluster (i.e. $r > 3.7$ arcmin).

Supplementing present data with the photoelectric photometry of bright stars by JS83, we have plotted the dereddened $V_o/(B–V)_o$ CMD for the stars in the cluster region in Fig. 18. The photometric

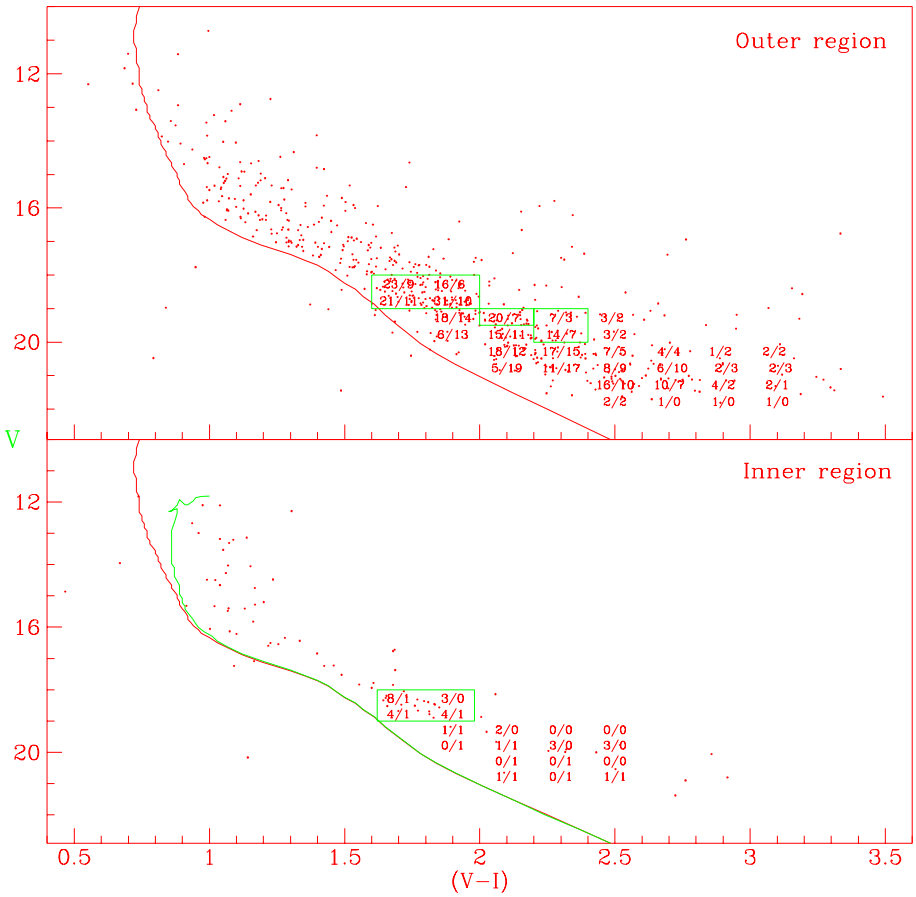

Figure 15. The statistics of stars in the NGC 654 cluster region (numerator) and in the field region (denominator). The box represents the locations of statistically significant number of probable PMS stars.

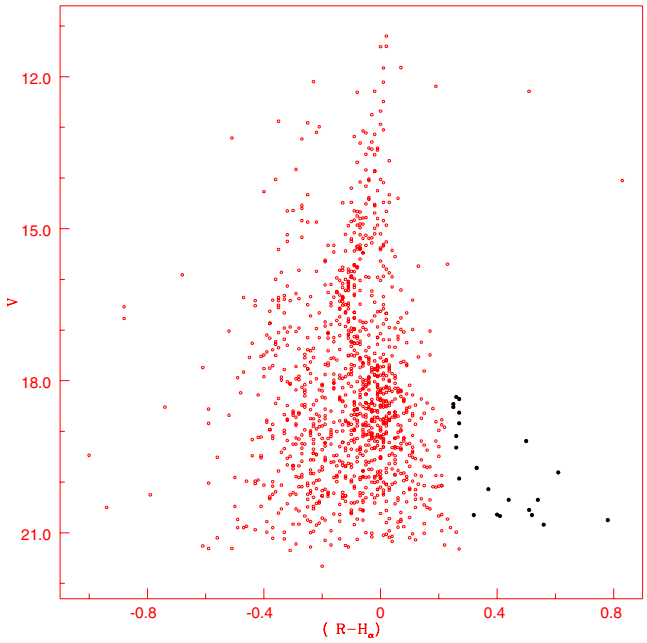

Figure 16. V, (R–Hα) diagram for the stars in the NGC 654 cluster region. The filled circles represent probable PMS stars with Hα emission.

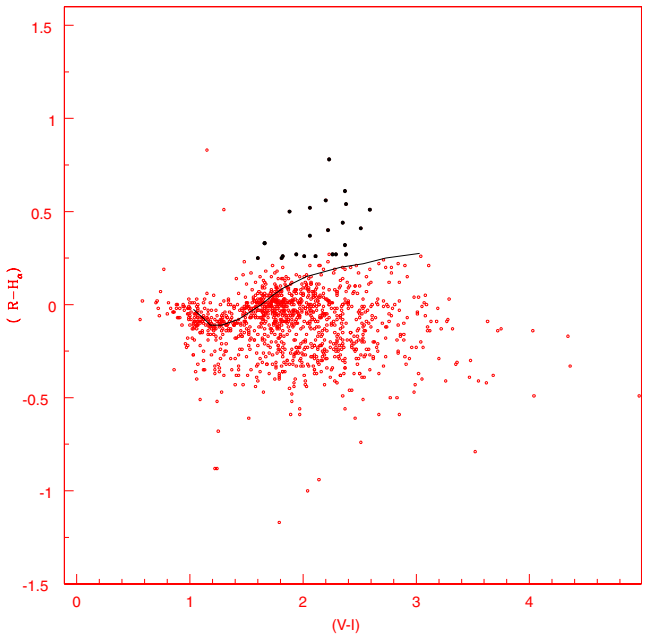

Figure 17. (R–Hα), (V–I) diagram for the stars in the NGC 654 cluster region. The filled circles represent probable PMS stars with Hα emission. The solid line represents the reddened normal MS relation for NGC 2264 (see text).

Table 10. Probable Hα emission stars in NGC 654.

No.	X	Y	V	$(B-V)$	$(V-I)$	$(R-\mathrm{H}\alpha)$	Radius (arcsec)
17	414.09	473.00	20.651	–	2.058	0.517	29.121
72	364.94	508.97	18.457	1.288	1.807	0.254	60.726
84	487.17	521.61	19.186	1.612	1.881	0.495	65.819
157	398.14	400.79	20.673	–	2.511	0.414	102.782
210	311.71	450.95	18.361	1.723	2.265	0.267	123.453
213	308.89	456.43	20.746	–	2.231	0.785	124.016
262	323.93	398.82	18.315	1.575	2.005	0.263	143.012
290	275.33	464.68	20.552	–	2.586	0.511	153.781
325	377.05	657.68	19.315	1.530	2.115	0.262	164.810
363	292.78	379.51	19.718	–	1.657	0.333	178.885
432	502.29	309.07	20.352	–	2.379	0.540	205.981
442	281.32	349.41	19.089	1.270	1.816	0.262	208.138
507	544.05	301.95	18.838	1.602	1.943	0.268	231.077
568	301.59	274.27	20.138	–	2.061	0.366	257.263
667	200.30	310.94	20.352	–	2.349	0.438	293.656
755	382.95	176.34	20.639	–	2.218	0.401	326.380
812	178.33	745.60	18.522	1.271	1.600	0.250	348.088
830	550.03	171.44	18.630	1.877	2.381	0.268	351.545
1253	183.18	105.03	20.840	1.806	2.205	0.564	463.118
1321	226.95	55.47	20.991	–	3.039	0.259	486.653
1420	72.96	902.39	19.932	1.944	2.294	0.268	534.649
1484	−8.57	915.17	19.807	2.041	2.372	0.609	600.291
1490	858.06	925.71	20.654	–	2.367	0.316	607.264

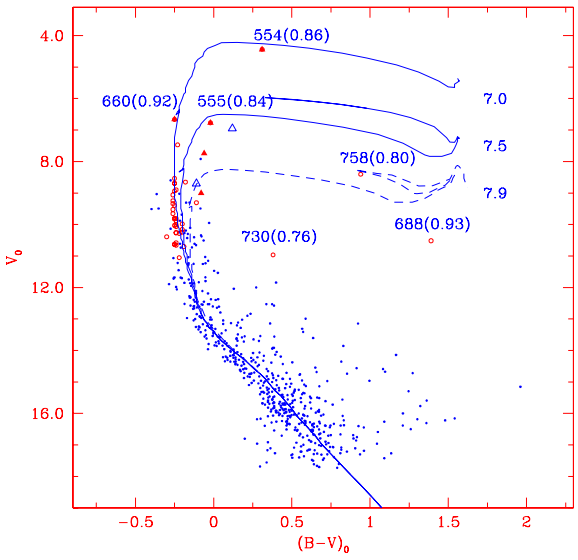

Figure 18. The dereddened V_o, $(B-V)_o$ CMD for the stars in the NGC 654 cluster region. The photometric observations, shown by open circles and triangles, were individually dereddened, whereas a mean value of $E(B-V) = 0.90$ was applied for present observations. The star numbers are taken from WEBDA. The isochrones for solar metallicity by Bertelli et al. (1994) for various ages have also been plotted. The numbers in parentheses represent membership probability. Filled and open triangles represent probable member stars and non-members, respectively, having polarization measurements.

observations, shown by open circles, were individually dereddened, whereas a mean value of $E(B-V) = 0.90$ was applied for present observations. Only the stars numbered (as per WEBDA; Mermilliod 1995) 554 and 555 lie within the boundary of the cluster (i.e. $r > 3.7$ arcmin), indicating a range of 10–32 Myr for the age of the cluster. We do not consider stars 688, 730 and 758 for age determination, although they have membership probability greater than 0.76 but they lie outside the boundary of the cluster obtained in the present work (i.e. $r > 3.7$ arcmin). If stars 688, 730 and 758, having membership probabilities 0.93, 0.76 and 0.80 respectively, are also cluster members, the cluster may have an even larger age spread. A distance modulus of 14.7 ± 0.10 was obtained. For a normal reddening law, this corresponds to 2.41 ± 0.11 kpc. The distance obtained in the present work is in good agreement with the distance (2.4 kpc) obtained by Stone (1980) and JS83 and slightly shorter than that obtained by PJ94 (2.69 kpc).

Stars having $V \geqslant 17.0$ ($M_V \sim 2.3$, mass $\sim$1.7 $M_\odot$) are on the PMS stage. The isochrones of 1- and 10-Myr PMS stars ($V/(B-V)$ from Iben 1965 and $V/(V-I)$ from Herbig & Dahm 2002) are also shown in Fig. 11. The distribution of PMS stars in Fig. 11 indicates an age spread of about 10 Myr. The overall scenario, i.e. the length of the MS up to $V \sim 17$ ($M_V \sim 2.3$) and the stars fainter than $V \sim 17$ mag, which require $\sim$10 Myr to reach the MS, are on the PMS stage, is consistent with the youngest component of the post-main-sequence stars having an age of $\sim$10 Myr. However, the evolutionary stage of the fainter stars is not consistent with the post-main-sequence stars having an age of $\geqslant$30 Myr.

8 MASS FUNCTION

The distribution of stellar masses at the time of birth of the cluster is known as the IMF. Studies of the IMF of star clusters are important to constrain star formation theories and also to understand the early stages of evolution of star clusters. The fundamental question about the IMF, whether the shape of the IMF is universal in time or space, is still open in spite of several detailed studies (see Scalo 1986, 1998). The most important contribution to the studies of the IMF is the advent of CCDs. CCDs combined with a moderate size telescope are giving deeper insights into low-mass stars, which can change the scenario of the IMF studies. One of the important studies was by Phelps & Janes (1993) who estimated the IMF for eight clusters with ages 10–70 $\times 10^6$. The slope of the MF they obtained varies from 0.4 to 1.8. However, some of the clusters in their sample (e.g. NGC 663), as pointed out by Scalo (1998), do not cover the entire cluster area. Pandey et al. (1992) have found that the nature of the MF does not remain the same over the entire region of the cluster and the slope of the MF steepens as the radial distances increase. In the present observations, we have imaged a sufficiently large area that covers the cluster including its coronal region where most of the low-mass stars are expected to be present.

With the help of CMDs, we can derive the observed LF of the probable MS cluster members and then the MF using the theoretical evolutionary model of Bertelli et al. (1994). As the IMF is the frequency distribution of stellar masses in an ensemble of newly formed stars in a stellar system or region, it is assumed safe to say that the IMF can be estimated for the young star clusters as they contain a nearly coeval set of stars formed from a parental cloud. However, the star formation in the present case as well as in the case of some other clusters (e.g. Pandey et al. 1990; Pandey, Ogura & Sekiguchi 2000; Pandey et al. 2001) is found to be a continuous process. Therefore, the term IMF cannot be strictly applicable in the case of NGC 663 and 654 and we can estimate only the present-day MF.

The MF is often expressed by the power law, $N(\log m) \sim m^{\Gamma}$ and the slope of the MF is given as

$$\Gamma = \mathrm{d}\log N(\log m)/\mathrm{d}\log m$$

Table 11. The MF of the clusters NGC 663 and 654. The numbers of probable cluster members (N) have been obtained after subtracting the expected contribution of field stars in each magnitude range. log ϕ represents log $N(\log m)$.

Cluster	Range	Mass	Mean	Inner region		Intermediate region		Outer region		Whole region	
	V (mag)	($M_\odot$)	log $M_\odot$	N	log ϕ	N	log ϕ	N	log ϕ	N	log ϕ
NGC 663	11–12	11.1–9.0	1.002	4.0	1.643	8.0	1.944	13.0	2.155	17.0	2.271
	12–13	9.0–6.6	0.892	22.0	2.213	42.0	2.494	49.0	2.561	71.0	2.722
	13–14	6.6–4.6	0.748	20.9	2.125	42.6	2.434	33.7	2.332	54.5	2.541
	14–15	4.6–3.1	0.586	32.7	2.281	77.8	2.657	114.5	2.825	147.1	2.934
	15–16	3.1–2.2	0.423	52.1	2.544	104.5	2.846	101.3	2.833	153.4	3.013
	16–17	2.2–1.6	0.279	59.5	2.634	167.5	3.083	326.6	3.373	386.0	3.446
	17–18	1.6–1.3	0.161	24.1	2.427	70.3	2.892	128.9	3.155	151.9	3.229
	18–19	1.3–1.1	0.079	38.3	2.723	77.9	3.031	477.7	3.819	516.0	3.852
NGC 654	11–12	11.5–9.7	1.025	1.0	1.131			3.0	1.609	4.0	1.733
	12–13	9.7–7.3	0.929	4.0	1.510			5.0	1.607	9.0	1.863
	13–14	7.3–5.1	0.792	5.9	1.576			6.7	1.633	12.6	1.906
	14–15	5.1–3.5	0.633	7.7	1.675			16.4	2.000	24.1	2.168
	15–16	3.5–2.4	0.470	7.4	1.655			30.6	2.270	38.0	2.365
	16–17	2.4–1.7	0.312	10.3	1.836			43.2	2.460	53.5	2.553
	17–18	1.7–1.4	0.190	5.6	1.822			35.7	2.627	41.4	2.690

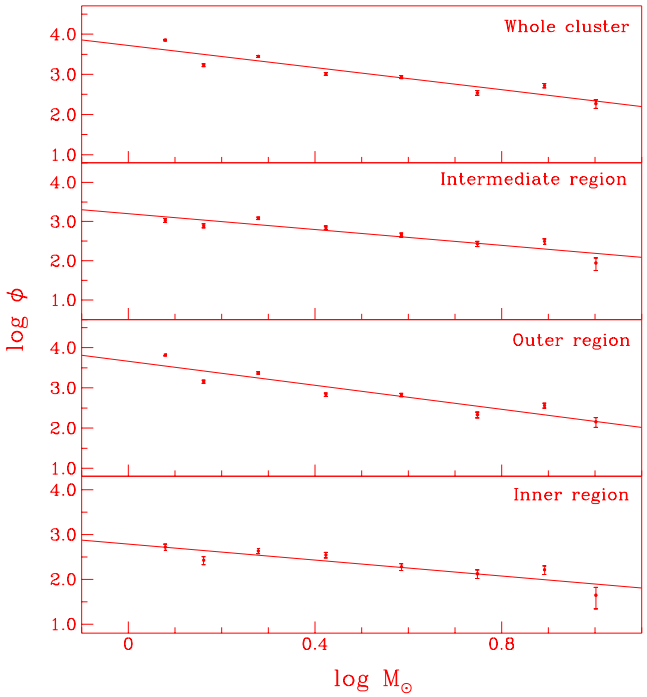

Figure 19. A plot of the MF in the various subregions of the cluster NGC 663. The error bars represent $1/\sqrt{N}$ errors.

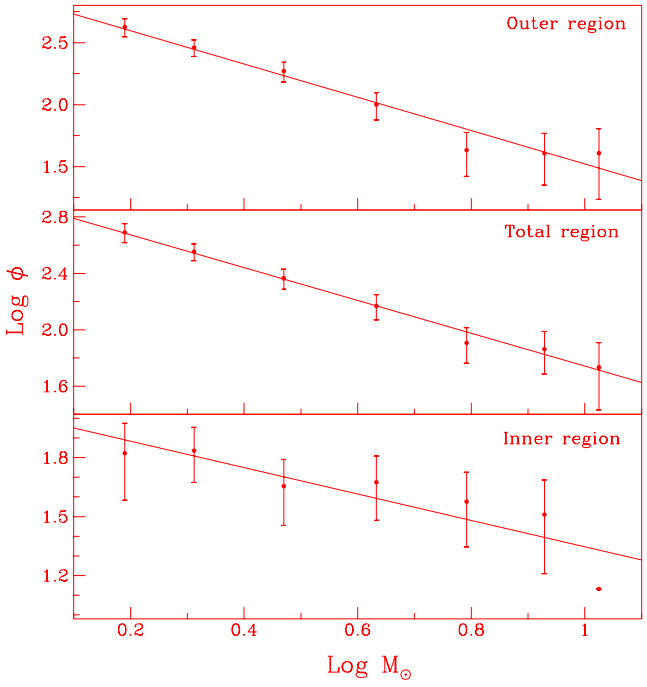

Figure 20. Same as Fig. 19, but for NGC 654.

where $N(\log m)$ is the number of stars per unit logarithmic mass interval. The classical value derived by Salpeter (1955) for the slope of IMF is $\Gamma = -1.35$. The LFs of the clusters NGC 663 and 654 (given in Table 9) have been converted to the MFs using the theoretical model of Bertelli et al. (1994) and the resultant MF data are given in Table 11. Figs 19 and 20 show plots of log N (log m) versus log m for NGC 663 and 654, respectively. Figs 19 and 20 manifest that the MF is not uniform in the whole cluster region, although it can be represented by a single power law for each subregion. The slopes of the MF for the subregions are given in Table 12, which indicates that the slope Γ becomes steeper as the radial distance increases. There is no indication for a truncation of the slope of the MF at the low-mass end ($\sim$1 $M_\odot$) as observed in the outer region of the cluster NGC 7654 (Pandey et al. 2001). However, the slope of the MF, Γ, for the entire cluster region of NGC 663 is -1.38 ± 0.22, which is similar to the Salpeter IMF ($\Gamma = -1.35$). For NGC 663, PJ94 and Kao, Chen & Hu (1998) have reported a shallower MF having $\Gamma = -1.06 \pm 0.05$ and $\Gamma = -0.77 \pm 0.20$, respectively. The MF slopes reported by PJ94 and Kao et al. (1998) are based on the observations of $\sim$20 $\times$ 20 arcmin^2 and $\sim$16 $\times$ 16 arcmin^2 field only. As we have discussed in Section 5, that the minimum extent of the cluster NGC 663 is $r \sim 17.5$ arcmin, the MF reported by PJ94 and Kao et al. (1998) does not represent the MF of the entire region of the cluster NGC 663. In the case of NGC 654, the slope of the

Table 12. The MF slope Γ in various subregions of the clusters NGC 663 and 654.

Cluster	Region	Mass range ($M_\odot$)	$\Gamma \pm \sigma$
NGC 663	Inner	1.1–11.1	-0.89 ± 0.20
	Inner	0.9–11.1	-0.87 ± 0.16
	Intermediate	1.1–11.1	-1.10 ± 0.18
	Outer	1.1–11.1	-1.50 ± 0.25
	Outer	0.9–11.1	-1.71 ± 0.25
	Whole	1.1–11.1	-1.38 ± 0.22
NGC 654	Inner	1.4–8.8	-0.67 ± 0.16
	Outer	1.4–8.8	-1.34 ± 0.12
	Whole	1.4–8.8	-1.16 ± 0.05

MF for the entire cluster region is -1.16 ± 0.05, which is slightly shallower than the Salpeter value.

9 MASS SEGREGATION

Mass segregation, in the sense that higher-mass stars are preferentially found towards the centre of the cluster, has been reported in many galactic star clusters as well as star clusters in the Large Magellanic Cloud (see, for example, Pandey et al. 1992, 2001; Fischer et al. 1998, and references therein). To characterize the degree of mass segregation in NGC 663, we subdivided the sample into three mass groups ($9.12 \geqslant M_\odot > 4.24$, $4.24 \geqslant M_\odot > 1.59$ and $1.59 \geqslant M_\odot \geqslant 0.95$), whereas for NGC 654 we subdivided the sample into the following three mass groups ($11.5 \geqslant M_\odot > 7.3$, $7.3 \geqslant M_\odot > 2.4$ and $2.4 \geqslant M_\odot \geqslant 1.2$). Figs 21 and 22 show the cumulative distribution as a function of radius in the three different mass groups of both the clusters. These normalized cumulative distributions are corrected for the incompleteness and the probable contamination due to the fact that field stars have also been removed. Figs 21 and 22 clearly indicate an effect of mass segregation in the cumulative distribution in the sense that most massive stars tend to lie near the cluster centre. The Kolmogorov–Smirnov test confirms the statement that the cumulative distribution of most massive stars in both

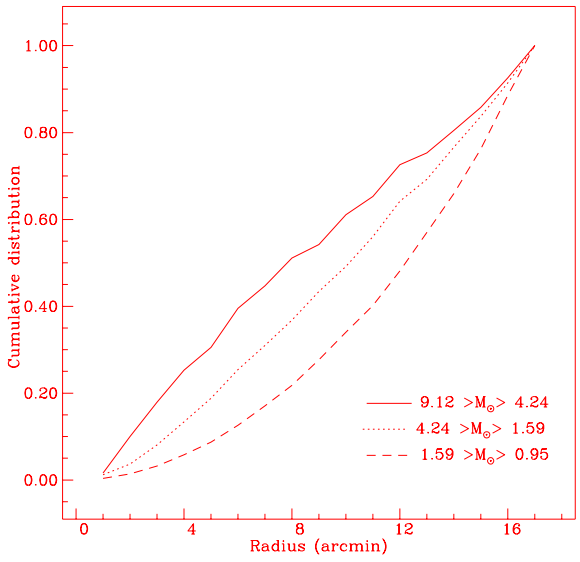

Figure 21. Cumulative distribution function for different mass intervals in the cluster NGC 663.

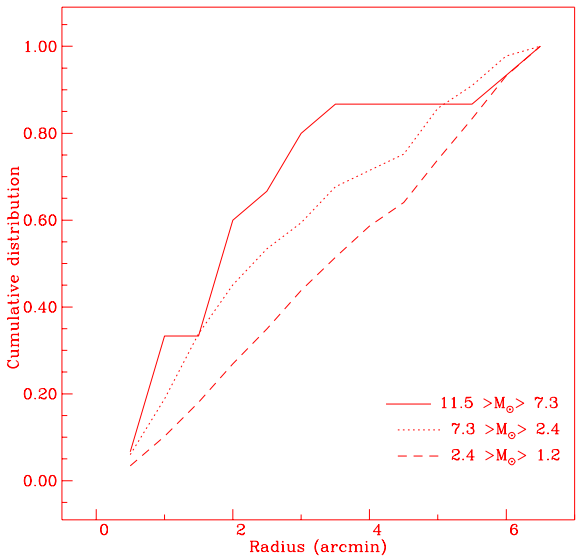

Figure 22. Same as Fig. 21, but for NGC 654.

clusters is different at a confidence level better than 99 per cent from that of relatively less massive stars.

We have estimated the relaxation time to decide whether the mass segregation discussed above is primordial or due to dynamical relaxation. Because of the dynamical relaxation, low-mass stars in a cluster may possess the largest random velocities, and consequently these will try to occupy a larger volume than high-mass stars (see Mathieu 1985; McNamara & Sekiguchi 1986; Mathieu & Latham 1986). The dynamical relaxation time, T_E, of the clusters can be estimated using the relation

$$T_E = \frac{8.9 \times 10^5 (N R_h^3/\bar{m})^{1/2}}{\log(0.4N)},$$

where N is the number of cluster members, R_h is the radius containing half of the cluster mass and $\bar{m}$ is the average mass of cluster stars (see Spitzer & Hart 1971). The estimated total number of MS stars and the total mass of the MS stars in the given mass range ($1.1 \leqslant M_\odot \leqslant 11.1$ for NGC 663; $1.4 \leqslant M_\odot \leqslant 8.8$ for NGC 664) are obtained with the help of the LF. This mass should be considered as a lower limit to the total mass of the cluster. For the half-mass radius, we used half of the cluster extent. Various parameters used to estimate the dynamical relaxation time T_E for both clusters are given in Table 13. Using these numbers, the relaxation time T_E obtained is also given in Table 13. In the case of NGC 663, the obtained relaxation time T_E is greater than the age of the cluster; therefore, we can conclude that the observed mass segregation is due to the star formation process itself. However, in the case of NGC 654, the estimated relaxation time is less than the age of the cluster, so the dynamical relaxation may also be a reason for the observed mass segregation in the cluster NGC 654.

Table 13. The dynamical relaxation time T_E and parameter used to estimate T_E for the clusters NGC 663 and 654.

Parameter	NGC 663	NGC 654
N	1498	305
R_h	6.15 pc	1.3 pc
$\bar{m}$	2.4 $M_\odot$	2.4 $M_\odot$
T_E	120 Myr	7 Myr
Age	13 Myr	20 Myr

10 DISCUSSION

The distribution of interstellar matter inside the clusters NGC 663 and 654 (see Section 6.2) indicates a slight lack of interstellar matter at the centre. In the case of very young clusters (e.g. NGC 3603 and 30 Dor), Pandey et al. (2000) and Brandl et al. (1996), respectively, have also found that the stars in the cores of these clusters show almost no reddening. A similar trend was also observed in the case of an intermediate-age cluster NGC 7654 (Pandey et al. 2001). Stellar winds or supernova explosions have been considered as a probable explanation for the lack of dust (and gas) at the centre of these clusters.

Photometric, spectroscopic and polarimetric observations indicate an anomalous reddening law in both clusters. However, the errors in the data are large and more infrared and polarimetric observations are needed to conclude about the size and behaviour of the dust grains present in these cluster regions.

Both clusters show an age spread of ∼15–20 Myr on the basis of post-main-sequence stars. The CMDs of NGC 663 show that the low-mass stars (∼1 $M_{\odot}$), which have a contraction time ∼50 Myr, are on the MS despite the fact that the cluster has a post-main-sequence age ∼13 Myr. On the other hand, NGC 654 shows a large number of stars on PMS stage with an age spread of ∼10 Myr. The star formation history in the cluster NGC 663 seems to support the conventional picture of star formation in clusters where 'low-mass stars' form first and that star formation continues over a long period of time. It is interesting to mention that the above scenario of star formation is in contradiction with that indicated by CMDs of the cluster NGC 654, which is situated at about the same distance as NGC 663 and about 35 pc away from NGC 663. The post-main-sequence stars in NGC 654 reveal an age of ∼10–32 Myr for the cluster, whereas PMS stars indicate an age of about 1–10 Myr; this suggests that the formation of low-mass stars does not cease after the formation of most massive stars. This scenario has been supported by recent observations of, for example, NGC 6611 (Hillenbrand et al. 1993), Tr14, Tr16 (DeGioia et al. 2001), several young clusters and OB associations (Massey, Johnson & De Giola-Eastwood 1995) and NGC 3603 (Pandey et al. 2000). The CMDs of NGC 654 also indicate that the post-main-sequence age of stars in the central region is greater than that of those in the outer region, which indicates that the star formation might have initiated in the central region of NGC 654.

In the NGC 654 region, we detected 22 stars showing Hα emission. Here, we have to keep in mind that, using the $(R–H\alpha)/(V–I)$ diagram, only stars with strong Hα emission could be detected, as most of the PMS stars show weak Hα emission. making their detection much harder (Preibisch & Zinnecker 1999). It is interesting to mention that out of 22 stars showing Hα emission, only three stars are located in the core of the cluster, nine are located in the outer region and the remaining 11 are located outside the boundary of the cluster (i.e. $r \leqslant 3.7$ arcmin). The statistics given (not corrected for incompleteness of the data) in Fig. 15 gives ∼20 and ∼70 probable PMS stars in the core and the outer region, respectively. This indicates that ∼15 and ∼13 per cent of the PMS stars in the core and the outer region, respectively, show evidence of Hα emission. All the PMS stars, in accordance with theory, should be surrounded by dusty circumstellar disc and usually produce Hα emission. What could be the reason for the absence of Hα emission in probable PMS stars? The following may be the possible explanation.

(i) They could be field stars. The MS MF of NGC 654 does not show truncation at the lower-mass end (∼1.4 $M_{\odot}$). The extrapolation of the MF for 1.4–1.0 $M_{\odot}$ as well as statistics given in Fig. 15 indicate a significant number of member stars in the mass range 1.4–1.0 $M_{\odot}$. Therefore, we exclude this possibility.

(ii) All the material surrounding PMS stars could be swept away by stellar winds from massive stars or supernova explosions. Such a possibility has been suggested to explain the lack of emission stars in NGC 6231 (Sung et al. 1998) and in the Upper Scorpius OB Associations (Preibisch & Zinnecker 1999). In such a scenario, the lack of reddening material near the cluster centre, as in the case of NGC 6231, is expected. In the case of NGC 654, it is found that the stars close to the centre are less reddened than those located in the outer region. Stellar winds or supernova explosions may be possible explanations for the lack of reddening material near the centre of NGC 654. If stellar winds or supernova explosions cause the removal of the surrounding material of PMS stars, then there should be fewer (percentage) Hα emission stars in the central region in comparison with the outer region. This is because the stars in the central region should be more affected by the stellar winds or supernova explosions, as most massive stars are found to be situated near the cluster centre. We do not observe such a type of spatial distribution of Hα emission stars. Therefore, we conclude that the stellar winds or supernova explosions may not be the reason for the absence of Hα emission in the PMS stars of NGC 654.

(iii) The large number of PMS stars identified by Hillenbrand et al. (1993) in NGC 6611, which showed no evidence of circumstellar material, led them to suggest that only 5 per cent of PMS stars ($2 < M_{\odot} < 5$) are active and show Hα emission. They concluded that disc survival times are much shorter than 1 Myr for intermediate- and high-mass stars. In the case of NGC 654, we found that ∼13 per cent PMS stars ($M < 1.7\ M_{\odot}$) show evidence of a circumstellar disc. A few stars having a PMS age ∼10 Myr show evidence of a circumstellar disc, which is in agreement with solar-type stars for which the disc lifetime is ∼10 Myr.

The MF of both clusters is not uniform over the entire region of the cluster. The slope of the MF becomes steeper in the outer region of the clusters. However, the MF in both clusters can be represented by a single power law without any evidence of truncation at the lower-mass end. The slope of the MF of the entire region of NGC 663 is similar to that of the Salpeter value, whereas in the case of NGC 654 it is shallower than the Salpeter value.

The above discussion indicates that star formation in star clusters is a continuous process that is highly localized and it depends on the prevailing conditions in different parts of the cloud/cluster.

11 SUMMARY AND CONCLUSION

The current paper is the continuation of the series in which we plan to carry out wide field CCD photometry around open clusters using the telescopes available at Kiso (Japan) and Nainital (India), to study in detail the structure, star formation history and MF of open clusters. A detailed study of two young open clusters, NGC 663 and 654, reveals the following.

(i) Supernovae explosion or stellar winds from massive stars may be a probable explanation for the lack of interstellar matter near the centre of both clusters.

(ii) There are indication for anomalous reddening law in both the clusters. More infrared/polarimetric observations are needed to conclude about the nature of the reddening law.

(iii) Both clusters are situated at about same distance (∼2.4 kpc).

(iv) In NGC 663, the star formation history indicates that the low-mass stars formed first and star formation continued over a

long period. Whereas the star formation history of NGC 654 reveals that formation of low-mass stars in the cluster does not cease after the formation of most massive stars. In the case of NGC 654, there is an indication that initial star formation might have started from the central region of the cluster.

(v) The MFs in both clusters can be represented by a single power law. There is no indication of truncation of the MF at the low-mass end. The MFs in both clusters become steeper in the outer region of the clusters. The slope of the MF, in the case of NGC 663, is similar to that given by Salpeter (1955), whereas, in the case of NGC 654, the MF slope is shallower than the Salpeter value.

(vi) Of the PMS stars with masses $M < 1.7$ $M_{\odot}$, only about 13 per cent show evidence for Hα emission due to circumstellar material.

ACKNOWLEDGMENTS

AKP is grateful to the Department of Science and Technology (DST), India, and to the Japan Society for the Promotion of Science (JSPS) for providing funds to visit Kiso Observatory to take observations. AKP is also grateful to the staff of Kiso Observatory for their generous help during the stay. The authors are grateful to the anonymous referee for useful comments.

REFERENCES

Bertelli G., Bressan A., Chiosi C., Fagotto F., Nasi E., 1994, A&AS, 106, 275
Brandl B. et al., 1996, ApJ, 466, 254
Davis L., Greenstein J. L., 1951, ApJ, 114, 206
DeGioia Eastwood K., Throop H., Walker G., Cudworth K. M., 2001, ApJ, 549, 578
Fischer P., Pryor C., Murray S., Mateo M., Richtler T., 1998, AJ, 115, 592
Fosalba P., Lazarian A., Prunet S., Tauber J. A., 2002, AJ, 564, 762
Greenberg J. M., 1968, in Middlehurst B. M., Allen L. H., eds, Stars and Stellar Systems Vol. 7, Nebulae and Interstellar Matter. University of Chicago Press, Chicago, p. 221
Herbig G. H., Dahm S. E., 2002, AJ, 123, 304
Hillenbrand L. A., 1997, AJ, 113, 1733
Hillenbrand L. A., Massey P., Strom S. E., Merril K. M., 1993, AJ, 106, 19 06
Hiltner W. A., 1956, ApJS, 1, 389
Hoag A. A., Johnson H. L., Iriarte B., Mitchell R. I., Hallam K. L., Sharpless S., 1961, in Publications of United States Naval Observatory, Second Series, Vol. XVII, Part 7 (H61)
Hsu J. C., Berger M., 1982, ApJ, 262, 732
Huestamendia G., del Rio G., Mermelliod J. C., 1993, A&AS, 100, 25
Iben I. Jr, 1965, ApJ, 141, 993
Jain S. K., Srinivasulu G., 1991, Opt. Eng., 30, 1415
Johnson H. L., Morgan W. W., 1953, ApJ, 117, 313
Joshi U. C., Sagar R., 1983, MNRAS, 202, 961 (JS83)
Kaluzny J., Udalski A., 1992, Acta Astron., 42, 29
Kao K.-C., Chen W.-P., Hu J.-Y., 1998, Chin. A&A, 22, 62
King I., 1962, AJ, 67, 471
Kroupa P., 2001, MNRAS, 322, 231
Landolt A. U., 1992, AJ, 104, 340
Leisawitz D., 1988, NASA Ref. Publ., 1202, 160
Leisawitz D., Bash F. A., Thaddeus P., 1989, ApJS, 70, 731
McCuskey S. W., Houk N., 1964, AJ, 69, 412
McMillan R. S., 1978, ApJ, 225, 880
McNamara B. J., Sekiguchi K., 1986, ApJ, 310, 613
Massey P., Johnson K. E., De Giola-Eastwood K., 1995, ApJ, 454, 151
Mathieu R. D., 1985, in Proc. IAU Symp. 113, Dynamics of Star Clusters. Reidel, Dordrecht, p. 427
Mathieu R. D., Latham D. W., 1986, AJ, 92, 1364
Mermilliod J. C., 1995, in Egret D., Abrecht M. A., eds, Information and On-line Data in Astronomy. Kluwer Academic, Dordrecht, p. 227
Moffat A. F. J., 1972, A&AS, 7, 355
Moffat A. F. J., Vogt N., 1974, Veroff des Astron. Institut der Ruhr-Universitat Bochum, 2, 1
Nilakshi, Sagar R., Pandey A. K., Mohan V., 2002, A&A, 383, 153
Pandey A. K., Mahara H. S., Sagar R., 1990, AJ, 99, 617
Pandey A. K., Mahara H. S., Sagar R., 1992, BASI, 20, 287
Pandey A. K., Ogura K., Sekiguchi K., 2000, PASJ, 52, 847
Pandey A. K., Nilakshi, Ogura K., Sagar R., Tarusawa K., 2001, A&A, 374, 504
Pandey A. K., Upadhyay K., Nakada Y., Ogura K., 2003, A&A, 397, 191
Pesch P., 1960, ApJ, 132, 696
Phelps R. L., Janes K. A., 1993, AJ, 106, 1870
Phelps R. L., Janes K. A., 1994, ApJS, 90, 31 (PJ94)
Pigulski A., Kopacki G., Kolaczkowski Z., 2001, A&A, 376, 144 (P01)
Preibisch T., Zinnecker H., 1999, AJ, 117, 2381
Sagar R., Yu Q. Z., 1989, MNRAS, 240, 551
Salpeter E. E., 1955, ApJ, 121, 161
Samson W. B., 1975, ApSS, 34, 363
Samson W. B., 1976, ApSS, 44, 217
Scalo J. M., 1986, Fund. Cosmic Phys., 11, 1
Scalo J. M., 1998, in Gilmore G., Parry I., Ryan S., eds, ASP Conf. Series, Vol. 142, Proc. of the 38th Herstmonceux meeting, The Stellar Initial Mass Function. Astron. Soc. Pac., San Francisco, p. 201
Serkowski K., 1997, in Gehrels T., ed. Proc. IAU Coll. 23, Planets, Stars and Nebulae studied with Photopolarimetry. Univ. Arizona Press, Tucson AZ, p. 135
Serkowski K., Mathewson D. S., Ford V. L., 1975, ApJ, 196, 261
Spitzer L. Jr, Hart M. H., 1971, ApJ, 164, 399
Stone R. C., 1980, PASP, 92, 426
Sung H., Bessel M. S., Lee S. W., 1998, AJ, 115, 734
Tapia M., Costero R., Echevarria J., Roth M., 1991, MNRAS, 253, 649
Turner D. G., 1976, AJ, 81, 1125
van den Bergh S., de Roux J., 1978, AJ, 83, 1075
Whittet D. C. B., van Breda I. G., 1978, A&A, 66, 57
Yadav R. K. S., Sagar R., 2001, MNRAS, 328, 370

This paper has been typeset from a TEX/LATEX file prepared by the author.